ACS OMEGA

Open Access

http://pubs.acs.org/journal/acsodf

Article

Synthesis and Characterization of a Novel DOPO-Based Flame Retardant Intermediate and Its Flame Retardancy as a Polystyrene Intrinsic Flame Retardant

Shaobo Dong,*,⊥ Yazhen Wang,*,⊥ Li Liu, Hongge Jia, Yu Zang, Liwu Zu, Tianyu Lan, and Jun Wang

Cite This: *ACS Omega* 2023, 8, 48825−48842

Read Online

ACCESS | Metrics & More | Article Recommendations

ABSTRACT: The research on intrinsic flame retardant has become a hot topic in the field of flame retardant. The synthesis of reactive flame-retardant monomer is one of the effective methods to obtain an intrinsic flame retardant. In addition, in view of the small molecular flame retardant easily migrates from the polymer during the use process, which leads to the gradual reduction of the flame retardant effect and even the gradual loss of flame retardant performance, and the advantages of atom transfer radical polymerization (ATRP) technology in polymer structure design and function customization, we first synthesized reactive flame retardant monomer 6-(hydroxymethyl)dibenzo[c,e][1,2]oxaphosphinine 6-oxide (FAA-DOPO), then synthesized polystyrene bromine (PS_{148}-Br) macromolecular initiator by ATRP technology, and finally obtained block copolymer polystyrene-*b*-poly{6-(hydroxymethyl)dibenzo-[c,e][1,2]oxaphosphinine 6-oxide} (PS-*b*-PFAA-DOPO) by the polymerization of FAA-DOPO initiated by macromolecular initiator PS_{148}-Br by ATRP technology. The chemical structure of FAA-DOPO was characterized by 1D and 2D NMR (^{1}H, ^{13}C, DEPT 135, HSQC, COSY, NOE, and HMBC) spectra, Fourier transform infrared spectroscopy (FTIR), liquid chromatography-tandem mass spectrometry (LC−MS) and X-ray photoelectron spectroscopy (XPS). The chemical structure and molecular weight of PS-*b*-PFAA-DOPO were characterized by FTIR and gel permeation chromatography (GPC). The thermal and flame-retardant properties of PS-*b*-PFAA-DOPO were characterized by thermogravimetry analysis (TG), UL-94, limiting oxygen index (LOI), and microscale combustion calorimetry (MCC). It was found that FAA-DOPO could be used as a monomer for polymerization, although FAA-DOPO had a large steric hindrance from the chemical structure of FAA-DOPO, the UL-94 grade of PS-*b*-PFAA-DOPO reached the V-0 grade, and the LOI increased by 59.12% compared with PS_{148}-Br.

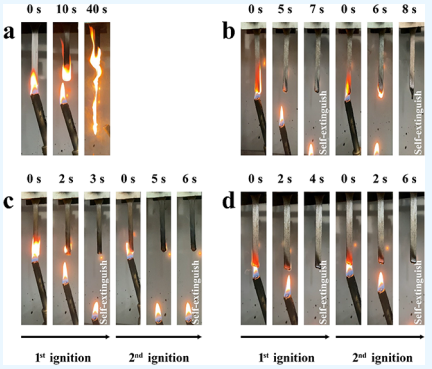

1. INTRODUCTION

Polystyrene, as one of the five general plastics, has the advantages of low density, good chemical resistance, low cost, and easy processing and is widely used in heat insulation, electrical, automobile, and other fields. However, polystyrene is easy to burn when heated, which will release toxic gases and a large amount of smoke, and can melt, drip, and flow in the combustion process, thus making the fire spread. Therefore, it is imperative to improve the flame retardant performance of polystyrene.[1−8] According to the flame retardant system, it mainly includes mineral flame retardant, halogen flame retardant, phosphorus flame retardant, silicone flame retardant, biobased flame retardant, and so on.[8−27] Among them, halogen flame retardants are all the rage, but they are prohibited because of their toxicity and bioaccumulation.[3,8,28−33] Phosphorus flame retardants have attracted much attention because of their excellent flame retardant efficiency and environmental friendliness, and have gradually become one of the research hotspots in today's society.[2,3,28,31−36] Phosphorus flame retardants mainly include ammonium polyphosphate, aluminum hypophosphite, 9,10-dihydro-9-oxa-10-phosphaphenanthrene 10-oxide (DOPO) and its derivatives.[3,9,31,33,37] Phosphorus flame retardants will produce phosphoric acid or similar substances during thermal degradation, which can inhibit the combustion process of the condensed phase. In addition, PO · radicals produced by phosphorus flame retardants have a gas phase flame retardant effect.[3,38,39]

Small molecular flame retardants easily escape from the polymer matrix during use, which leads to the gradual loss of flame retardancy or even loss of flame retardancy. In addition, due to the poor compatibility between polymer matrix and additives, the flame retardant effect will also be affected.[33] In

Received: August 22, 2023
Revised: November 22, 2023
Accepted: November 24, 2023
Published: December 13, 2023

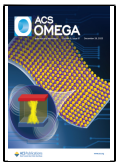

Scheme 1. Synthesis Route for FA-DOPO, FAA-DOPO, PS-Br, and PS-*b*-PFAA-DOPO

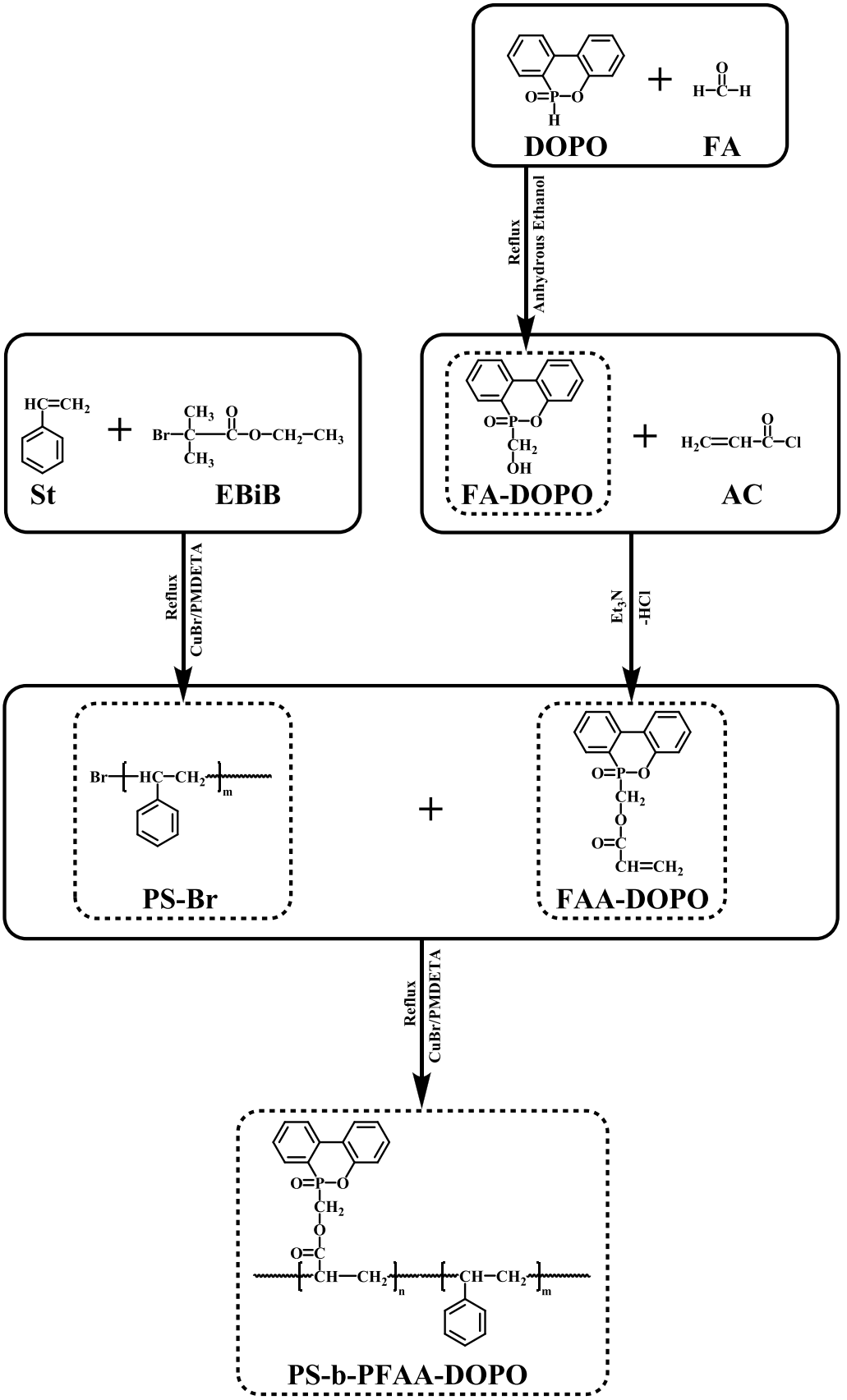

view of this, flame retardants gradually develop from blend additive flame retardants to reactive flame retardants and intrinsic flame retardants.[3,40,41] Among them, the flame retardant substances are introduced into the polystyrene

https://doi.org/10.1021/acsomega.3c06235
ACS Omega 2023, 8, 48825−48842

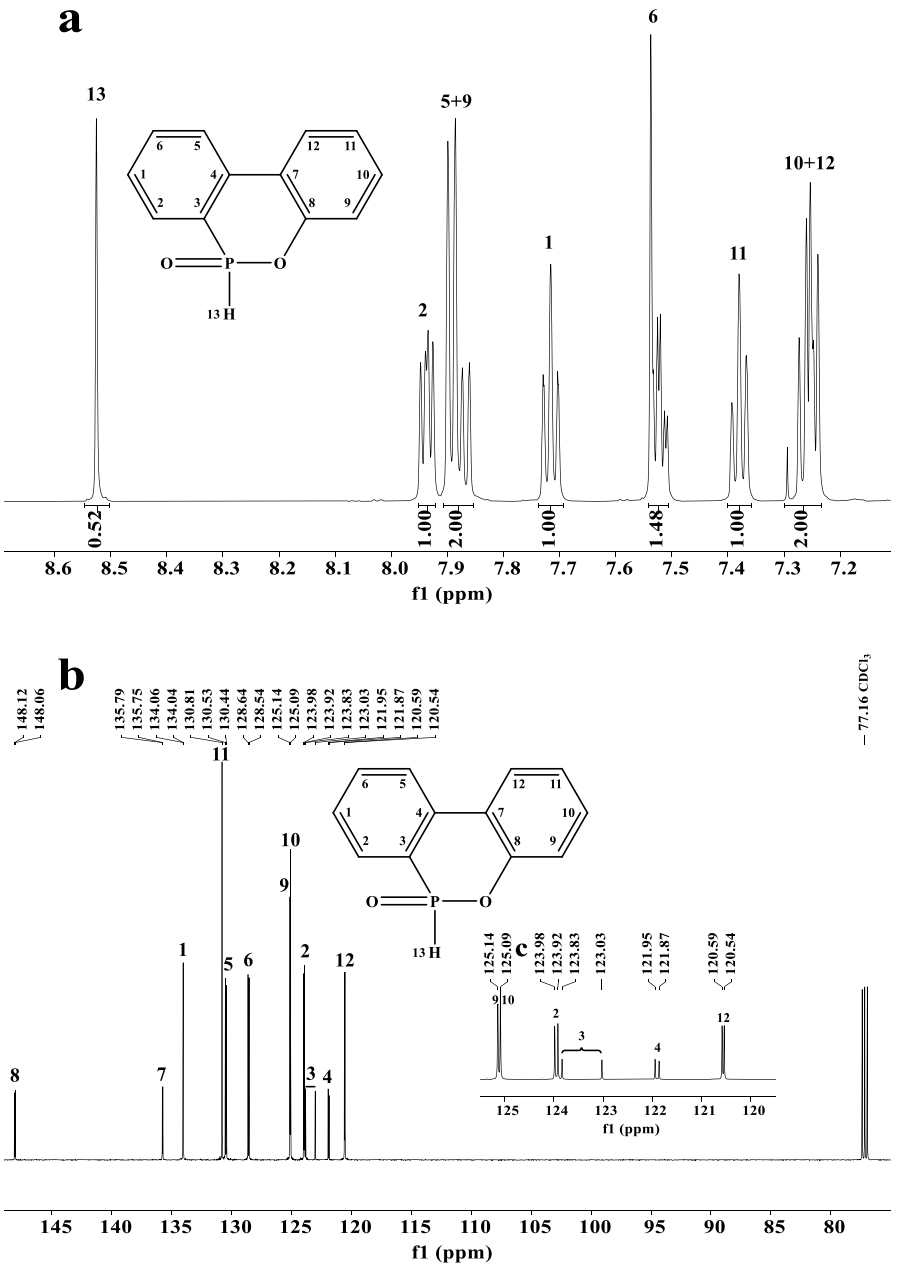

Figure 1. ^{1}H NMR (a) and ^{13}C NMR (b) spectra of DOPO, illustration c is a partially enlarged view of Figure b.

molecular chain by polymerization, and the flame retardant groups often do not escape from the polymer matrix during polymer processing or polymer use, which ensures the long-term stability of the flame retardant properties. However, the selection of suitable comonomers often becomes the main factor limiting the development of this method.[3,19,42,43]

In the aspect of molecular structure design,[35] especially reversible inactivation radical polymerization technology, it is possible to obtain polymer flame retardants with complex structure, determined molecular weight, and low dispersion.[37,41,44,45] In view of the wide application of DOPO in flame retardant field[22,46−61] and the urgent demand for functional monomers with flame retardant function in the flame retardant field, our research group synthesized a functional monomer FAA-DOPO from DOPO, and characterized its structure in detail. In addition, in order to prove that FAA-DOPO can be used for copolymerization with polystyrene, our research group designed the flame retardant molecule by the ATRP method, synthesized PS-*b*-PFAA-DOPO with intrinsic flame retardants, and studied its flame retardant performance.

2. EXPERIMENTAL SECTION

2.1. Materials. Styrene (St, 99%, AR), 9,10-dihydro-9-oxa-10-phosphaphenanthrene 10-oxide (DOPO, 97%, AR), formaldehyde aqueous solution (FA, 37%, AR), acetonitrile (ACN, 99.5%, AR), anhydrous ethanol (99.5%, AR), triethylamine (TEA, 99%, AR), acryloyl chloride (AC, 96%, stabilized with 200 ppm of 4-methoxyphenol, AR), N,N-dimethylformamide (DMF, 99.5%, AR), ethyl α-bromoisobutyrate (EBiB, 98%, AR), N,N,*N*′,*N*″,*N*″-pentamethyldiethylenetriamine (PMDETA, 99%, AR), acetic acid (99.5%, AR),

https://doi.org/10.1021/acsomega.3c06235
ACS Omega 2023, 8, 48825−48842

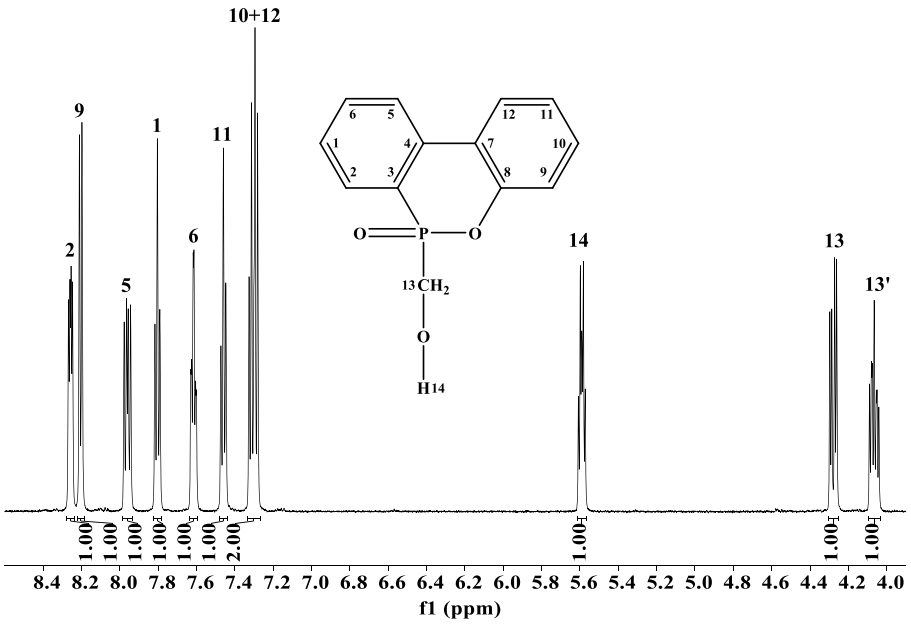

Figure 2. ^{1}H NMR spectra of FA-DOPO.

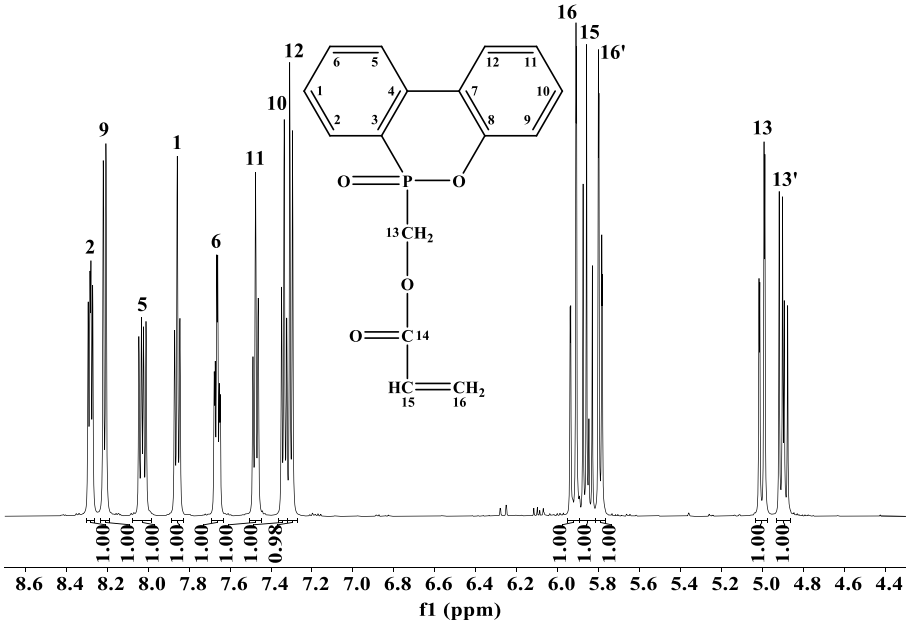

Figure 3. ^{1}H NMR spectra of FAA-DOPO.

and cuprous bromide (CuBr, AR) were purchased from Shanghai Aladdin Biochemical Technology Co., Ltd. CuBr was purified with acetic acid before use. All other chemicals were used as received without further purification.

2.2. Instruments. 1D and 2D NMR (^{1}H, ^{13}C, DEPT 135, HSQC, COSY, NOE, and HMBC) spectra were recorded with a Bruker AVANCE (600 MHz) spectrometer, using $CDCl_3$ (^{1}H, 7.26 ppm, ^{13}C, 77.16 ppm) or DMSO-d_6 (^{1}H, 2.50 ppm, ^{13}C, 39.52 ppm) as an internal standard.

Fourier transform infrared (FTIR) spectra were recorded with a PerkinElmer Spectrum One B spectrometer using KBr pellets. Spectra in the range of 4000−450 cm^{-1} were obtained by 32 scans at a resolution of 4 cm^{-1}.

Thermo U3000 UPLC and Thermo Q-Exactive Orbitrap MS were used to determine the relative molecular masses of the chemical compounds.

X-ray photoelectron spectra (XPS) were recorded with a Thermo ESCALAB250Xi spectrometer using Al K_α exciton radiation ($h\nu$ −5000 eV).

The number-averaged molar mass ($\bar{M}_n$) and polydispersity index (PDI) were determined with a Wyatt GPC/SEC-MALS instrument equipped with a DAWN 8 laser light scattering detector and an Optilab T-Rex refractive index detector using DMF (0.5 mL/min) with 0.1 M LiBr as the mobile phase at 50 °C, and polystyrene standards with narrow distributions were used for calibration.

The limiting oxygen index (LOI) measurement was carried out with a JF-3 oxygen index measurement instrument

https://doi.org/10.1021/acsomega.3c06235
ACS Omega 2023, 8, 48825−48842

Table 1. Analysis of ^{1}H NMR Spectra of FAA-DOPO

δ_H (ppm)	number of hydrogen atoms	type of splitting peak	J (Hz)
8.28	1	dd	8.2, 5.1
8.21	1	dd	8.1, 1.6
8.03	1	ddd	13.5, 7.6, 1.4
7.89−7.83	1	m	
7.66	1	td	7.5, 3.0
7.48	1	td	7.5, 6.7, 1.3
7.34	1	td	7.7, 1.3
7.30	1	dd	8.1, 1.3
5.92	1	dd	17.0, 1.9
5.85	1	dd	17.0, 10.2
5.79	1	dd	10.2, 1.9
5.00	1	dd	14.8, 2.5
4.90	1	dd	14.8, 10.0

according to the GB/T2406.2-2009 testing procedure with a sample size of 100 × 10 × 4 mm (length × width × thickness).

Microscale combustion calorimetry (MCC) tests were carried out on a FAA-PCFC microcalorimeter instrument. The sample was heated to 700 °C from room temperature at a heating rate of 1 °C/s under oxygen flows of 20 mL/min.

Vertical burning tests (UL-94) were carried out with a M607 UL-94 instrument according to GB/T2408-2021. The dimensions of specimens were 125.0 × 13.0 × 3.0 mm (length × width × thickness).

2.3. Synthesis of 6-(Hydroxymethyl)dibenzo[c,e]-[1,2]oxaphosphinine-6-oxide (FA-DOPO). A certain amount of DOPO was added to the two-neck round-bottom flask, a magnetic stirring rotor was put into the two-neck round-bottom flask, and a certain amount of anhydrous ethanol was measured and added into the two-neck round-bottom flask. A certain amount of formaldehyde solution was measured and added to a constant pressure-dropping funnel, which was connected to the grinding mouth of the two-neck round-bottom flask. The molar ratio of DOPO to formaldehyde was 1:1. The middle grinding mouth of the two-neck round-bottom flask was connected to a condenser tube. The assembled reaction device was placed in an oil bath at 85 °C. When the solution in the two-neck round-bottom flask became a uniform transparent solution, the valve of the constant pressure dropping funnel was opened to add formaldehyde solution to the two-neck round-bottom flask drop by drop. After 8 h of reaction, the reaction was stopped, and a granular white precipitate was formed at the bottom of the flask. The precipitate was filtered while it was hot. After washing with anhydrous ethanol, deionized water, and filtration many times, the collected white powder was dried overnight in an oven at 80 °C for the next experiment.

2.4. Synthesis of FAA-DOPO. A certain amount of FA-DOPO synthesized in the previous step was added into the two-neck round-bottom flask, a magnetic stirring rotor was put into the two-neck round-bottom flask, and a certain amount of acetonitrile was added into the two-neck round-bottom flask. The middle grinding port of the two-neck round-bottom flask was connected with a condenser tube, and the other grinding port of the two-neck round-bottom flask was sealed with a rubber stopper. The assembled reaction device was placed in an ice water bath and stirred for 6 h. A certain amount of triethylamine was injected into the two-neck round-bottom flask through the rubber stopper and stirred in the ice water bath for another 1 h. Then a certain amount of acryloyl chloride was injected into the two-neck round-bottom flask through the rubber stopper. The molar ratio of FA-DOPO to acryloyl chloride was 1:1. With the addition of acryloyl chloride, the solution in the two-neck round-bottom flask gradually changed from white to light yellow. After acryloyl chloride was added into the two-neck round-bottom flask, the reaction mixture was continuously stirred at room temperature for another 12 h. After the reaction was finished, the reaction mixture was filtered to remove the precipitate triethylamine hydrochloride to obtain the filtrate. The filtrate was distilled under reduced pressure by a rotary evaporator to obtain a yellow viscous substance. The obtained viscous yellow substance was separated by column chromatography to obtain a light-yellow powdered FAA-DOPO, which was reserved for the next experiment.

2.5. Synthesis of Macroinitiator PS-Br by ATRP. Polystyrene macromolecular initiator (PS-Br) was synthesized by ATRP technology according to the molar ratio of monomer to initiator of 100:1 and the molar ratio of catalyst CuBr, ligand PMDETA, and initiator EBiB of 1:3:1 with DMF as the solvent. The synthesis process of PS-Br is shown in Scheme 1. PMDETA, EBiB, styrene, CuBr, and DMF were added into a three-neck round-bottom flask, and the grinding mouths of the three-neck round-bottom flask were sealed with a turnaround rubber stopper. Two syringe needles were inserted into the turnaround rubber stoppers of the two grinding mouths of the three-neck round-bottom flask respectively, and bubble high-purity nitrogen through syringe needles with needles below the liquid level for 1 h to remove oxygen in the reaction system. Then, the syringe needles were quickly pulled out and the needle holes were sealed with vacuum silicone grease. The reaction device was reacted in an oil bath at 100 °C for 3 h. After the reaction mixture is precipitated by ethanol, washed by ethanol, washed by deionized water, and filtered, the collected white powder is dried overnight in an oven for further experiment.

2.6. Synthesis of PS-*b*-PFAA-DOPO by ATRP with PS-Br as a Macromolecular Initiator. The synthesis of the PS-*b*-PFAA-DOPO diblock copolymer with PS-Br as a macromolecular initiator by the ATRP method is similar to that of PS-Br by the ATRP method. The molar ratios of FAA-DOPO to PS-Br were 50:1, 100:1, and 200:1, respectively. The molar ratio of catalyst CuBr, ligand PMDETA, and macromolecular initiator PS-Br was 1:3:1. PMDETA, PS-Br, FAA-DOPO, CuBr, and DMF were added

https://doi.org/10.1021/acsomega.3c06235
ACS Omega 2023, 8, 48825−48842

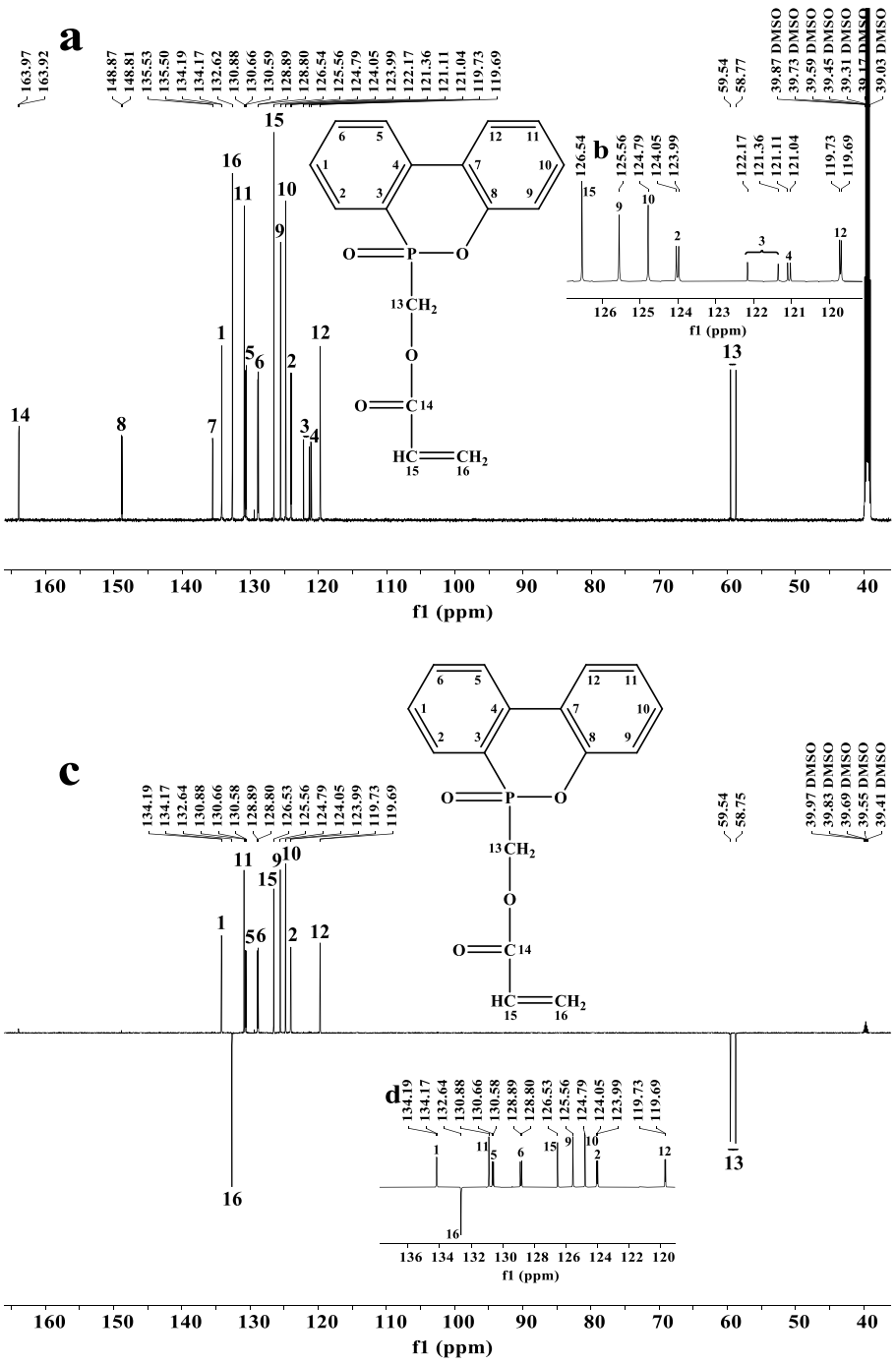

Figure 4. ^{13}C NMR (a) and DEPT 135 (c) spectra of FAA-DOPO, illustrations b and d are partially enlarged views of figure a and c, respectively.

into a three-neck round-bottom flask, and the grinding mouths of the three-neck round-bottom flask were sealed with a turnaround rubber stopper. Two syringe needles were inserted into the turnaround rubber stoppers of the two grinding mouths of the three-neck round-bottom flask, respectively, and bubble high-purity nitrogen was through syringe needles with needles below the liquid level for 1 h to remove oxygen in the reaction system. Then, the syringe needles were quickly pulled out and the needle holes were sealed with vacuum silicone grease. The reaction device was reacted in an oil bath at 100 °C for 3 h. After the reaction mixture is precipitated by ethanol, washed by ethanol, washed by deionized water, and filtered, the collected white powder is dried overnight in an oven for further experiment.

2.7. Preparation of Test Spline. PS-Br and PS-*b*-PFAA-DOPO synthesized with different molar ratios of FAA-DOPO and PS-Br were added into the mold, and the mold was placed in a vacuum oven, vacuumized, kept at 175 °C for 3 h, and naturally cooled to room temperature to obtain test splines.

3. RESULTS AND DISCUSSION

3.1. Structural Characterization of FAA-DOPO. *3.1.1. NMR Analysis.* In order to characterize the structure

https://doi.org/10.1021/acsomega.3c06235
ACS Omega 2023, 8, 48825−48842

Table 2. Comprehensive Analysis of ^{13}C NMR, DEPT-135, and HSQC of FAA-DOPO

δ_C (ppm)	$\overline{\delta}_C$ (ppm)[a]	$\delta_{C\text{-DEPT-135}}$ (ppm)	number of carbon atoms	type of carbon atom	δ_H of directly connected hydrogen atoms (ppm)
163.97, 163.92	163.95		1	C	
148.87, 148.81	148.84		1	C	
135.53, 135.50	135.51		1	C	
134.19, 134.17	134.18	134.19, 134.17	1	CH	7.85
132.62	132.62	132.64	1	CH_2	5.92, 5.79
130.88	130.88	130.88	1	CH	7.48
130.66, 130.59	130.62	130.66, 130.58	1	CH	8.03
128.89, 128.80	128.84	128.89, 128.80	1	CH	7.66
126.54	126.54	126.53	1	CH	5.85
125.56	125.56	125.56	1	CH	8.21
124.79	124.79	124.79	1	CH	7.34
124.05, 123.99	124.02	124.05, 123.99	1	CH	8.28
122.17, 121.36	121.76		1	C	
121.11, 121.04	121.07		1	C	
119.73, 119.69	119.71	119.73, 119.69	1	CH	7.30
59.54, 58.77	59.15	59.54, 58.76	1	CH_2	5.00, 4.90

[a]The average value of chemical shifts of two spectral lines in which phosphorus causes coupling splitting of carbon spectra.

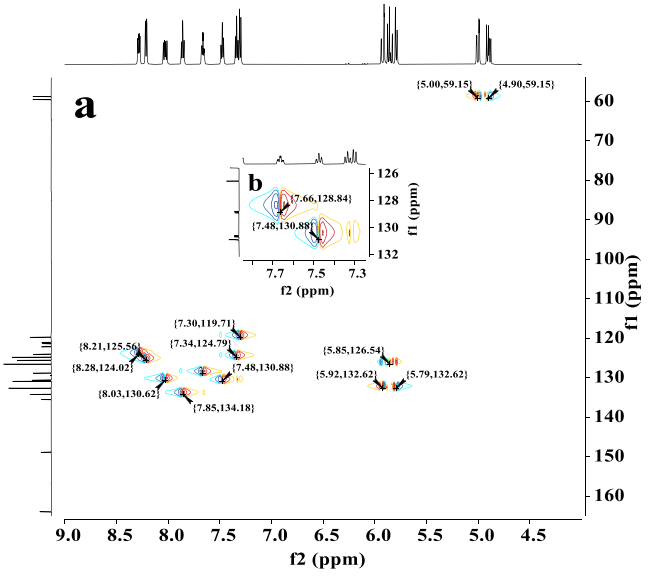

Figure 5. HSQC spectra of FAA-DOPO, illustration b is a partially enlarged view of figure a.

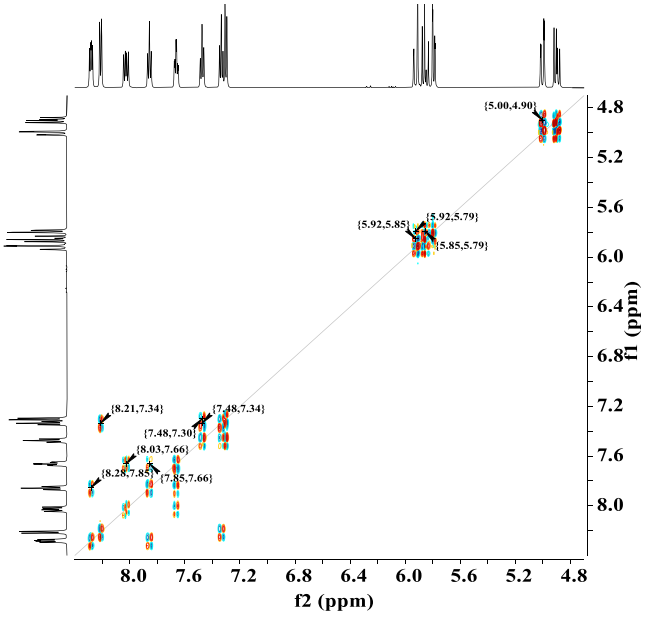

Figure 6. $^1H-^1H$-COSY spectra of FAA-DOPO.

of FAA-DOPO, ^1H and ^{13}C NMR were performed on the initial raw material DOPO. The results are shown in Figure 1a, b, respectively. It can be seen from NMR spectra that phosphorus (single isotope composition, 31P, spin quantum number 1/2) can split the spectral lines of the carbon spectrum (1J 40−150 Hz, 2J 5−10 Hz, and long-range coupling constants across more chemical bonds). Due to hydrogen being decoupled in carbon spectrum mapping, the coupling splitting caused by phosphorus cannot be removed. Phosphorus also splits the related peak groups in the hydrogen spectrum, because the splitting of the hydrogen spectrum is often complicated, so the splitting caused by phosphorus may not be obvious. However, the spectral lines of the carbon spectrum are clear, and the splitting of phosphorus is remarkable. The hydrogen proton chemical shift data in Figure 1a are as follows: ^1H NMR (600 MHz, $CDCl_3$): δ 8.53 (s, 1H), 7.94 (dd, J = 8.1, 5.1 Hz, 1H), 7.88 (ddd, J = 15.2, 7.7, 1.5 Hz, 2H), 7.74−7.69 (m, 1H), 7.54−7.51 (m, 1H), 7.38 (tt, J = 7.6, 1.4 Hz, 1H), 7.30−7.23 (m, 2H). The chemical shift at δ = 8.53 is attributed to the active hydrogen proton (P-*H*) on DOPO, and chemical shifts at δ = 7.23−7.94 are attributed to the hydrogen proton in the phenanthrene ring of DOPO. The position of the chemical shift peak of the ^{13}C NMR spectrum is shown in Figure 1b, and **Illustration 1**c is a partially enlarged view of Figure 1b for clearer observation.

As an intermediate, FA-DOPO was characterized by ^1H NMR (Figure 2). The hydrogen proton chemical shift data in Figure 2 are as follows: ^1H NMR (600 MHz, DMSO): δ 8.26 (dd, J = 8.2, 4.5 Hz, 1H), 8.20 (d, J = 7.9 Hz, 1H), 7.96 (dd, J = 12.8, 7.5 Hz, 1H), 7.80 (t, J = 7.8 Hz, 1H), 7.62 (td, J = 7.4, 2.8 Hz, 1H), 7.46 (t, J = 7.7 Hz, 1H), 7.34−7.27 (m, 2H), 5.59 (dt, J = 9.1, 5.8 Hz, 1H), 4.28 (dd, J = 15.1, 6.1 Hz, 1H), 4.07 (ddd, J = 14.7, 8.4, 5.6 Hz, 1H). The chemical shifts of δ = 4.07 and 4.28 are attributed to $-CH_2-$, the chemical shift of δ = 5.59 is attributed to O−*H*, and the chemical shifts of δ = 7.27−8.26 are attributed to

https://doi.org/10.1021/acsomega.3c06235
ACS Omega 2023, 8, 48825−48842

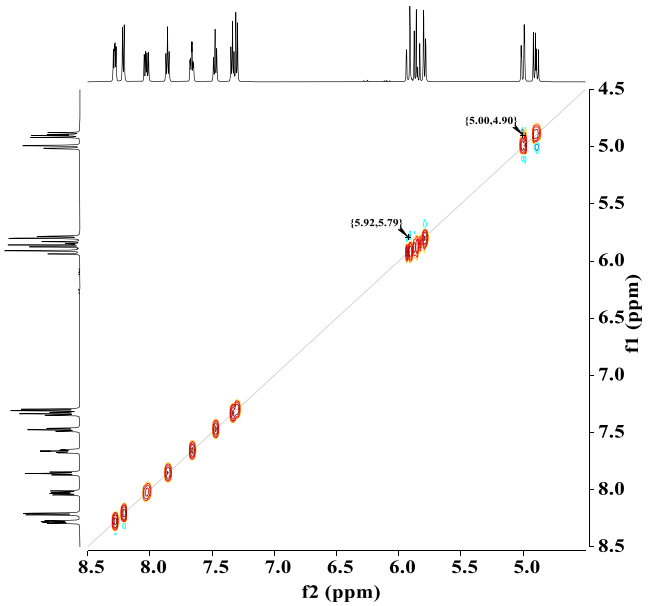

Figure 7. NOE spectra of FAA-DOPO.

Table 3. Analysis of ^{1}H−^{1}H-COSY Spectra of FAA-DOPO

δ_H (ppm)	δ_H of coupled hydrogen atoms (ppm)
8.28	7.85
8.21	7.34
8.03	7.66
7.85	8.28, 7.66
7.66	8.03, 7.85
7.48	7.34, 7.30
7.34	8.21, 7.48
7.30	7.48
5.92	5.85, 5.79
5.85	5.92, 5.79
5.79	5.92, 5.85
5.00	4.90
4.90	5.00

Table 4. Analysis of NOE Spectra of FAA-DOPO

δ_H (ppm)	δ_H of NOE-related hydrogen atoms (ppm)
5.92	5.79
5.00	4.90

phenanthrene hydrogen protons of FA-DOPO, and due to the influence of chemical environment, the chemical shift of phenanthrene hydrogen proton in FA-DOPO moves slightly to low field compared with that in DOPO.

Next, we focus on the NMR spectra of the synthesized flame retardant monomer FAA-DOPO. The ^{1}H NMR spectra of FAA-DOPO are shown in Figure 3. The chemical shifts, splitting peak types, and coupling constants of the ^{1}H NMR spectra of FAA-DOPO are listed in Table 1. The chemical shifts of δ = 4.90 and 5.00 are attributed to $-CH_2-$, the chemical shifts of δ = 5.79, 5.85, 5.92 are attributed to $-CH{=}CH_2$, and the chemical shifts of δ = 7.30−8.28 are attributed to phenanthrene hydrogen protons of FAA-DOPO, and due to the influence of chemical environment, the chemical shift of phenanthrene proton in FAA-DOPO moves slightly to low field compared with that in FA-DOPO.

To further confirm the chemical structure of the FAA-DOPO, the positions of the chemical shift peaks in the ^{13}C NMR spectra of the FAA-DOPO are shown in Figure 4a, **Illustration 4**b is a partially enlarged view of Figure 4a, the positions of the chemical shift peaks in the DEPT 135 spectra of the FAA-DOPO are shown in Figure 4c, and **Illustration 4**d is a partially enlarged view of Figure 4c for a clearer view. The NMR data in Figure 4 are shown in Table 2. According to the DEPT 135 spectra, the peaks of the carbon atoms connected with an odd number of hydrogen protons are upward, the peaks of the carbon atoms connected with an even number of hydrogen protons are downward, and the carbon atoms not connected with hydrogen protons are not peaked. By comparing ^{13}C NMR data with DEPT 135 data, it can be seen that δ = 163.97, 163.92, 148.87, 148.81, 135.53, 135.50, 122.17, 121.36, 121.11, 121.04 correspond to quaternary carbon atoms and are paired splitting peaks, δ = 132.62, 59.54, 58.77 correspond to secondary carbon atoms, and δ = 59.54 and 58.77 are paired splitting peaks.

In order to further determine the structure of the compound, we used 2D NMR spectra for further study. Figures 5−8 show HSQC, ^{1}H−^{1}H-COSY, NOE, and HMBC spectra of FAA-DOPO, respectively. Based on the data of 2D NMR spectra, the correlations between hydrogen proton and hydrogen proton and between hydrogen proton and carbon atom in FAA-DOPO are listed in Tables 2−5, respectively. For clearer observation, **Illustration 5**b is a partially enlarged view of Figure 5a, and Figure 8b is a partially enlarged view of Figure 8a.

Finally, the corresponding relationship between the chemical structure (Figure 9) of FAA-DOPO and NMR spectra is listed in Table 6 according to the data in Tables 1−5. Thus, NMR spectra strongly confirm the chemical structure of FAA-DOPO.

3.1.2. FTIR Analysis. The FTIR spectra of DOPO, FA-DOPO, and FAA-DOPO are shown in Figure 10. By comparing the FTIR spectra of DOPO, FA-DOPO, and FAA-DOPO, the results show that the O−H bond in FA-DOPO appears at 3310 cm^{-1}, which is formed by the reaction of DOPO with formaldehyde, and FA-DOPO does not have a P−H bond at 2385 cm^{-1}, indicating that DOPO has all reacted and FA-DOPO is obtained. In FAA-DOPO formed by the reaction of FA-DOPO with acryloyl chloride, the C=O bond appears at 1734 cm^{-1}, the C=C bond appears at 1623 cm^{-1}, the C−O−C bond appears at 1204 cm^{-1}, and there is no O−H bond in FAA-DOPO at 3310 cm^{-1}, which indicates that FA-DOPO has been completely reacted and FAA-DOPO has been obtained. FTIR results show that FA-DOPO and FAA-DOPO have specific functional groups that FA-DOPO and FAA-DOPO should have. That is to say, FTIR results show that FA-DOPO and FAA-DOPO have been successfully synthesized.

3.1.3. LC−MS Analysis. Figure 11 shows the LC−MS of FA-DOPO and FAA-DOPO. It can be observed that the main mass-to-charge ratio (m/z) peak of FA-DOPO is at 269.0332, which is due to FA-DOPO (m/z = 246.0446) obtaining one Na^+. In addition, the mass-to-charge ratio (m/z) peak of FA-DOPO at 247.0514 is due to FA-DOPO (m/z = 246.0446) obtaining one H^+. It can be observed that the main mass-to-charge ratio (m/z) peak of FAA-DOPO is at 323.0437, which is due to FAA-DOPO (m/z = 300.0551) obtaining one Na^+. In addition, the mass-to-charge ratio ($m/$

https://doi.org/10.1021/acsomega.3c06235
ACS Omega 2023, 8, 48825−48842

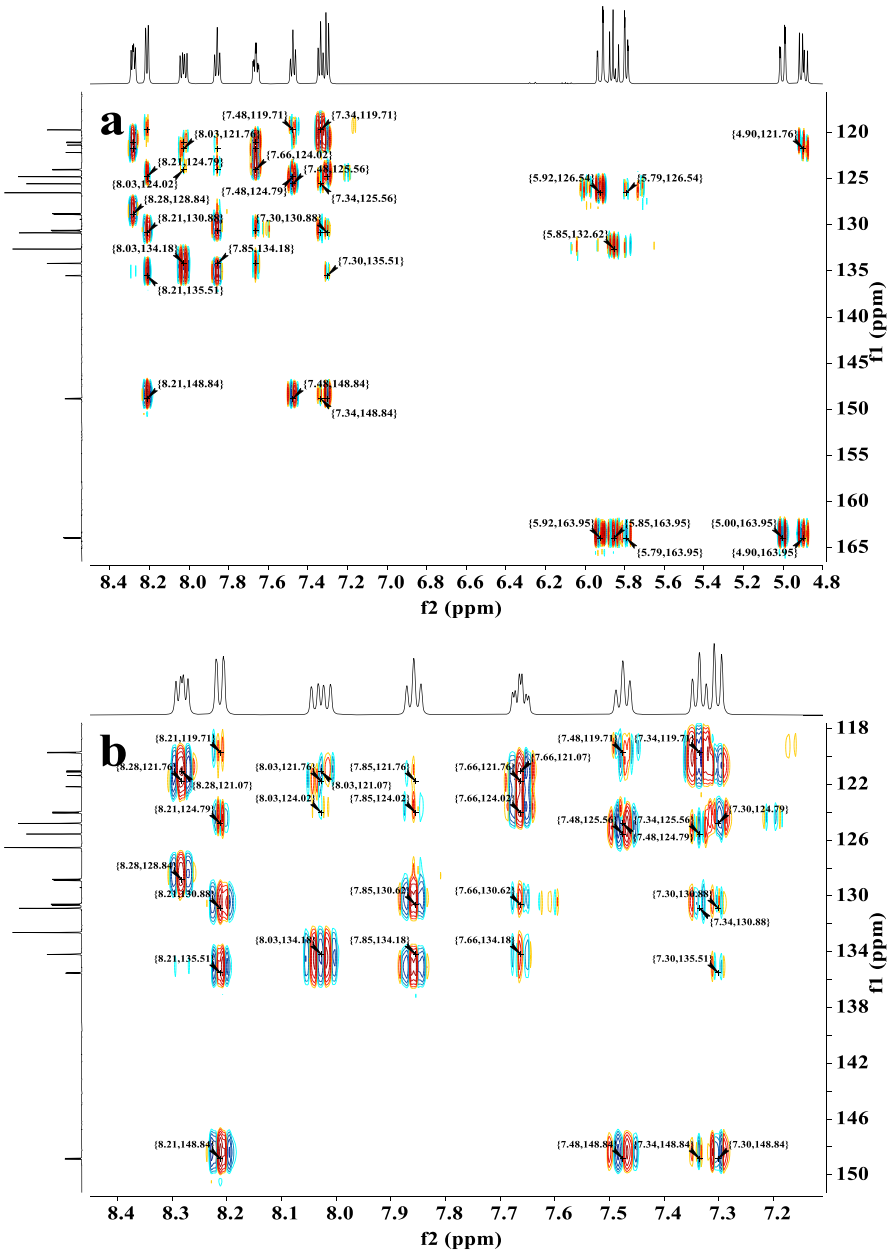

Figure 8. HMBC spectra of FAA-DOPO, figure b is a partially enlarged view of figure a.

z) peak of FAA-DOPO at 301.0619 is due to FAA-DOPO (m/z = 300.0551) obtaining one H^+. The results of LC-MS indicate the successful synthesis of FA-DOPO and FAA-DOPO.

3.1.4. XPS Analysis. Figure 12 shows the XPS spectra of FAA-DOPO and peak fitting of C 1s, O 1s, and P 2p. XPS of FAA-DOPO shows the existence of phosphorus at 132.08 eV, carbon at 283.08 eV, and oxygen at 531.08 eV (Figure 12a), and the corresponding results are listed in Table 7. Moreover, there are four binding states of carbon in the C 1s spectrum of FAA-DOPO (Figure 12b), centering at 283.02, 283.15, 284.7, and 287.35 eV, which is the characteristic peaks for the $=CH_2$, 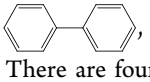 , P-CH_2−O/=HC and 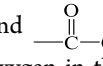 , respectively. There are four binding states of oxygen in the O 1s spectrum of FAA-DOPO (Figure 12c), centering at 529.76, 530.58, 531.5, and 532.01 eV, which are the characteristic peaks for the P=O, C=O, P−O, and C−O−C, respectively. There is one binding state of phosphorus in the P 2p spectrum of FAA-DOPO (Figure 12d), centering at 131.72 eV, which is the characteristic peak for the  .

The peak fitting results of C 1s show that the peak area percentage of the fitting peak corresponding to each group is consistent with the proportion of the corresponding group in the chemical structure of FAA-DOPO. In addition, the corresponding area percentages of O 1s and P 2p peaks are also consistent with the corresponding group percentages in the chemical structure of FAA-DOPO. Thus, XPS spectra strongly confirm the chemical structure of FAA-DOPO.

In summary, according to the analysis results of 1D and 2D NMR (^1H, ^{13}C, DEPT 135, HSQC, COSY, NOE, and HMBC) spectra, FTIR, LC−MS, and XPS, FAA-DOPO has been successfully synthesized and its chemical structure has

https://doi.org/10.1021/acsomega.3c06235
ACS Omega 2023, 8, 48825−48842

Table 5. Analysis of HMBC Spectra of FAA-DOPO

δ_C (ppm)	δ_H of long-range coupled hydrogen atoms (ppm)	δ_H of ^1J-coupled hydrogen atom (ppm)
163.97, 163.92	5.92, 5.85, 5.79, 4.90, 5.00	
148.87, 148.81	8.21, 7.48, 7.34, 7.30	
135.53, 135.50	7.30, 8.21	
134.19, 134.17	8.03, 7.66	7.85
132.62	5.85	
130.88	8.21, 7.30, 7.34	
130.66, 130.59	7.85, 7.66	
128.89, 128.80	8.28	
126.54	5.92, 5.79	
125.56	7.48, 7.34	
124.79	8.21, 7.48, 7.30	
124.05, 123.99	8.03, 7.85, 7.66	
122.17, 121.36	8.28, 8.03, 7.85, 7.66, 4.90	
121.11, 121.04	8.28, 8.03, 7.66	
119.73, 119.69	8.21, 7.34, 7.48	
59.54, 58.77		

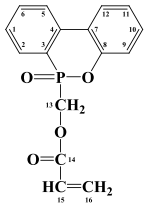

Figure 9. Chemical Structure of FAA-DOPO.

been strongly confirmed. Its chemical structure is shown in Figure 9.

3.2. Structural Characterization of PS-*b*-PFAA-DOPO.

3.2.1. FTIR Analysis. The FTIR spectra of PS-Br and PS-*b*-PFAA-DOPO are shown in Figure 13. For better comparison, the FTIR spectra of FAA-DOPO in Figure 10 are listed again in Figure 13. The results show that in PS-*b*-PFAA-DOPO, there are not only the characteristic peaks of C═O at 1734 cm^{-1} belonging to FAA-DOPO but also three groups of characteristic peaks at 1602, 1493, and 1452 cm^{-1} belonging to the benzene ring. There is no C═C bond belonging to the styrene monomer in the chemical structure of PS-Br, and there is no C═C bond belonging to the FAA-DOPO monomer in the chemical structure of PS-*b*-PFAA-DOPO, which indicates that both styrene monomer and FAA-DOPO monomer have taken addition polymerization.

3.2.2. GPC Analysis. The GPC trace of PS-Br macroinitiator and PS-*b*-PFAA-DOPO are shown in Figure 14, and the corresponding number-average molecular weight and PDIs are also labeled in Figure 14. The results of GPC analysis showed that the molecular weight of PS-*b*-PFAA-DOPO increased with the increase of the molar ratio of FAA-DOPO to macroinitiator PS-Br, which was mainly due to the fact that the molecular weight of polymer increased with the increase of the molar number of monomers when the molar number of initiator, polymerization time and polymerization temperature were the same. The number of structural units in PS-Br was calculated according to the GPC test results and the molecular weight of each structural unit in the polymer. According to the GPC test results, the number-average molecular weight of PS-Br is 15,640 g/mol. As can be seen from Scheme 1, the total molar mass (15,444.95 g/mol) of styrene structural units in macroinitiator PS-Br is obtained by subtracting the molecular weight of EBiB (195.05 g/mol)

Table 6. Correspondence between the Chemical Structure and NMR Spectra of FAA-DOPO

atomic number	type of carbon atom	δ_C (ppm)	$\overline{\delta}_C$ (ppm)[a]	δ_H (ppm)
1	CH	134.19, 134.17	134.18	7.85
2	CH	124.05, 123.99	124.02	8.28
3	C	122.17, 121.36	121.76	
4	C	121.11, 121.04	121.07	
5	CH	130.66, 130.59	130.62	8.03
6	CH	128.89, 128.80	128.84	7.66
7	C	135.53, 135.50	135.51	
8	C	148.87, 148.81	148.84	
9	CH	125.56	125.56	8.21
10	CH	124.79	124.79	7.34
11	CH	130.88	130.88	7.48
12	CH	119.73, 119.69	119.71	7.30
13	CH_2	59.54, 58.77	59.15	5.00, 4.90
14	C	163.97, 163.92	163.95	
15	CH	126.54	126.54	5.85
16	CH_2	132.62	132.62	5.92, 5.79

[a]The average value of chemical shifts of two spectral lines in which phosphorus causes coupling splitting of carbon spectra.

https://doi.org/10.1021/acsomega.3c06235
ACS Omega 2023, 8, 48825−48842

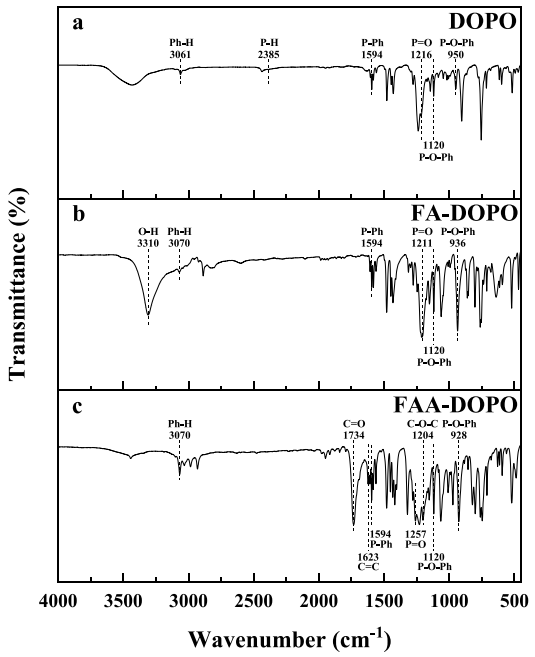

Figure 10. FTIR spectra of DOPO (a), FA-DOPO (b), and FAA-DOPO (c).

from the number-average molecular weight of macroinitiator PS-Br. The ratio of the total molar mass of styrene structural units to the molar mass of styrene (104.15 g/mol) is the number of styrene structural units in the macroinitiator PS-Br, so there are 148 styrene monomer units in the macromolecular chain of the macroinitiator PS-Br, so the macroinitiator PS-Br is named PS_{148}-Br. The number of styrene monomer units in the PS-*b*-PFAA-DOPO macromolecular chain is as much as that in the PS_{148}-Br macromolecular chain. In addition, the number-average molecular weight of PS-*b*-PFAA-DOPO minus the number-average molecular weight of PS_{148}-Br is the total molar mass of the FAA-DOPO block structural units. Therefore, the total molar mass of FAA-DOPO units in the macromolecular chain of PS-*b*-PFAA-DOPO synthesized with PS_{148}-Br and FAA-DOPO at molar ratios of 1:50, 1:100, and 1:200 are 9,640, 15,100, and 23,930 g/mol, respectively. The ratio of the total molar mass of FAA-DOPO units to the molar mass of FAA-DOPO (300.25 g/mol) is the number of FAA-DOPO units in the macromolecular chain of PS-*b*-PFAA-DOPO. Therefore, the number of FAA-DOPO units in the macromolecular chain of PS-*b*-PFAA-DOPO synthesized with PS_{148}-Br and FAA-DOPO at molar ratios of 1:50, 1:100, and 1:200 are 32, 50 and 80, respectively. Therefore, PS-*b*-PFAA-DOPO synthesized with PS_{148}-Br and FAA-DOPO at molar ratios of 1:50, 1:100, and 1:200 are named PS_{148}-*b*-PFAA-$DOPO_{32}$, PS_{148}-*b*-PFAA-$DOPO_{50}$ and PS_{148}-*b*-PFAA-$DOPO_{80}$, respectively.

3.3. Thermal Stability of PS-*b*-PFAA-DOPO. The thermal stability of PS-*b*-PFAA-DOPO was verified by TG

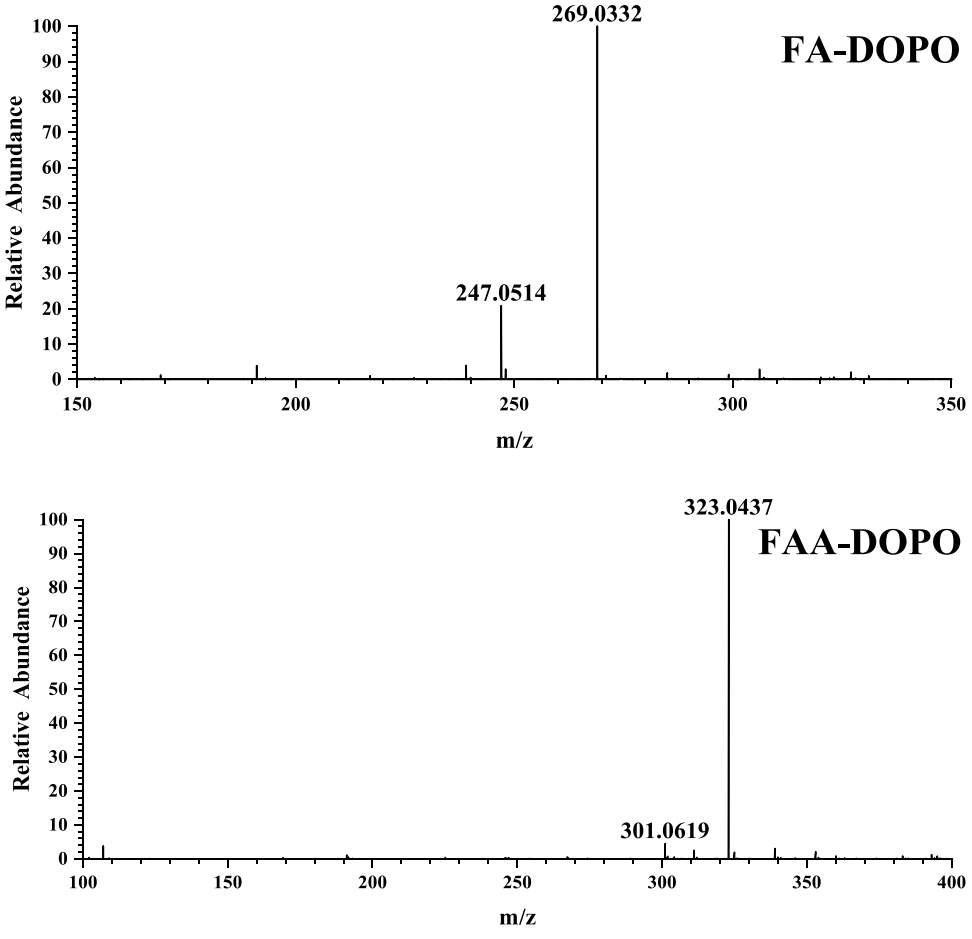

Figure 11. LC-MS of FA-DOPO and FAA-DOPO.

https://doi.org/10.1021/acsomega.3c06235
ACS Omega 2023, 8, 48825−48842

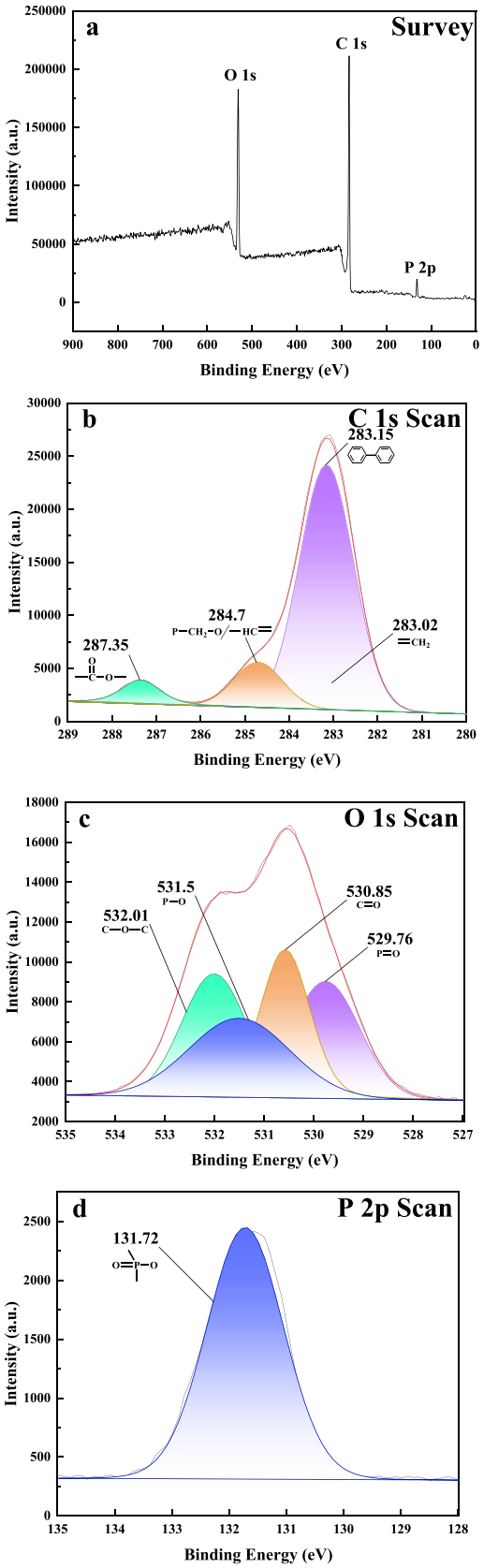

Figure 12. XPS spectra of FAA-DOPO: wide-scan spectra (a) of FAA-DOPO, C 1s (b), O 1s (c), and P 2p (d) core-level high-resolution spectra of FAA-DOPO, respectively.

Table 7. Correspondence of XPS Peak Fitting Electron Binding Energy Data of FAA-DOPO with Characteristic Functional Groups in Its Structure

Items	Functional group	Peak position, eV	Percentage of area, %
C 1s	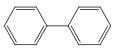	283.15	75%
	$=CH_2$	283.02	6.25%
	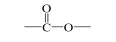	287.35	6.25%
	$P-CH_2-O/-HC=$	284.7	12.5%
O 1s	P−O	531.5	25%
	P=O	529.76	25%
	C−O−C	532.01	25%
	C=O	530.58	25%
P 2p	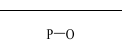	131.72	100%

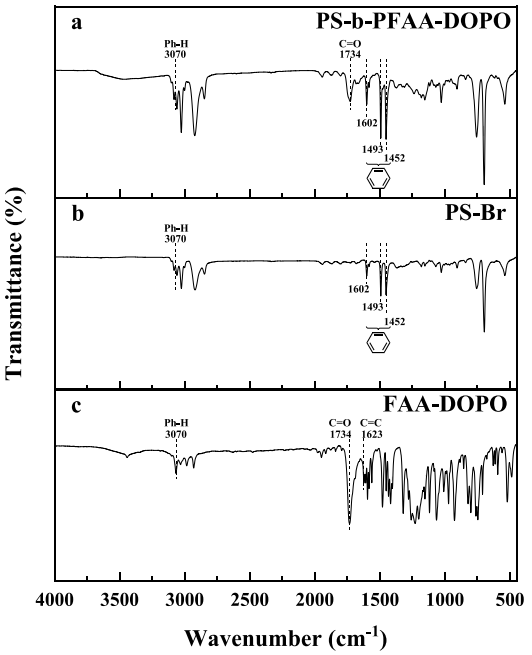

Figure 13. FTIR spectra of PS-*b*-PFAA-DOPO (a), PS-Br (b), and FAA-DOPO (c).

analysis under a nitrogen atmosphere. The TG and DTG curves are shown in Figure 15. As we can see from Figure 15, PS_{148}-Br undergoes one-stage thermal degradation via complex random scissions of molecular chains yielding styrene monomers and oligomers or their derivatives in the nitrogen atmosphere.[62] This process led to the formation of a small quantity of char residues (1.36 wt %). FAA-DOPO and PS-*b*-PFAA-DOPO undergo two-stage thermal degradation in the nitrogen atmosphere, and the first thermal degradation process occurs between 183−322 °C, mainly due to the breakage of ester bonds and gradual decomposition. The second stage thermal degradation of FAA-DOPO, PS_{148}-*b*-$PFAA\text{-}DOPO_{32}$, and PS_{148}-*b*-$PFAA\text{-}DOPO_{50}$ occurred at 322−471 °C, except for PS_{148}-*b*-$PFAA\text{-}DOPO_{80}$ which occurred at 322−419 °C. This was mainly due to the breakage of the phenanthrene ring structure and the opening of P═O and P−O chemical bonds, which produced PO· and

https://doi.org/10.1021/acsomega.3c06235
ACS Omega 2023, 8, 48825−48842

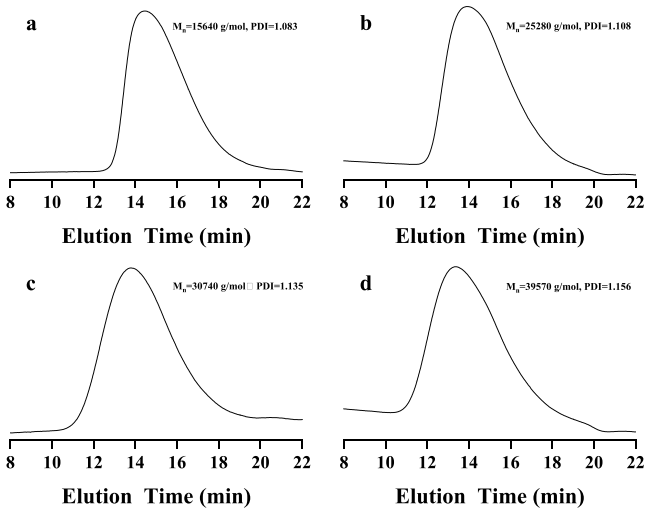

Figure 14. GPC trace of PS-Br macroinitiator (a) and PS-*b*-PFAA-DOPO synthesized with PS-Br and FAA-DOPO at molar ratios of 1:50 (b), 1:100 (c), and 1:200 (d).

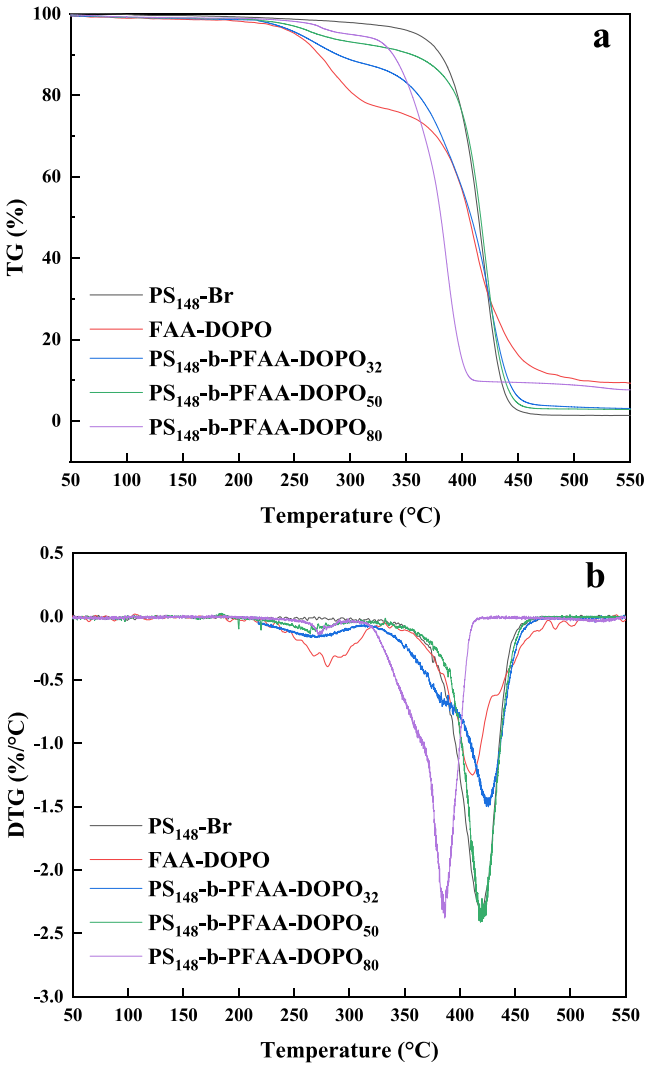

Figure 15. TG (a) and DTG (b) of PS_{148}-Br, FAA-DOPO, PS_{148}-*b*-PFAA-$DOPO_{32}$, PS_{148}-*b*-PFAA-$DOPO_{50}$, and PS_{148}-*b*-PFAA-$DOPO_{80}$.

PO_2· radicals and trapped carbon radicals produced during polystyrene macromolecular chains thermal degradation and prevented further degradation of molecular chains. Therefore, the increase of carbon residue was attributed to the generation of PO· and PO_2· radicals and the capture of carbon radicals (such as benzyl radicals produced during polystyrene macromolecular chains thermal degradation), thus limiting the random breakage of polystyrene macromolecular chains. The TG curve shows that the presence of FAA-DOPO blocks in PS-*b*-PFAA-DOPO reduces the mass loss rate; that is, the presence of FAA-DOPO blocks reduces the decomposition rate of polystyrene macromolecular chains. The lower degradation rate means that the release rate of combustible gas pyrolysis products is lower, which leads to a decrease in pHRR (Table 9). The curve in Figure 15 and the data in Table 8 shows that the initial degradation temperature of PS-*b*-FAA-DOPO ($T_{5\%}$, the temperature at which 5 wt % weight loss occurs) is lower than that of PS_{148}-Br. Based on the above analysis, it is verified again that the existence of the DOPO chemical structure makes the degradation process of PS-*b*-FAA-DOPO start earlier than that of PS_{148}-Br, and the degradation products are mainly released into the gas phase.[63−68]

3.4. Flame Retardancy of PS-*b*-PFAA-DOPO. UL-94 vertical burning and limiting oxygen index (LOI) tests are important for evaluating the flame retardancy of certain materials.[33] Figure 16 shows the UL-94 vertical combustion of PS_{148}-Br and PS-*b*-PFAA-DOPO. As shown in Figure 16a, once ignited, PS_{148}-Br burns rapidly, accompanied by a large amount of smoke, and fails to reach any UL-94 level. As shown in Figure 16b, PS_{148}-*b*-PFAA-$DOPO_{32}$ self-extinguishes quickly after generating a weak flame at the first ignition, and PS_{148}-*b*-PFAA-$DOPO_{32}$ self-extinguishes quickly after generating a slightly larger flame than the first ignition at the second ignition. The combustion time of PS_{148}-*b*-PFAA-$DOPO_{32}$ is significantly shortened (<10s) than that of PS_{148}-Br, and only a small amount of smoke is generated during combustion, reaching the V-0 level of UL-94. As shown in Figure 16c, PS_{148}-*b*-PFAA-$DOPO_{50}$ self-extinguished quickly after a small flame appeared at the first ignition, and PS_{148}-*b*-PFAA-$DOPO_{50}$ self-extinguished quickly after a slightly smaller flame appeared than the first ignition at the second ignition. In addition, the combustion time of PS_{148}-*b*-PFAA-$DOPO_{50}$ is significantly shortened (<10s) than that of PS_{148}-Br, and only a small amount of smoke is generated during combustion, reaching the V-0 level of UL-94. As shown in Figure 16d, PS_{148}-*b*-PFAA-$DOPO_{80}$ self-extinguished quickly after a faint flame appeared at the first ignition, and PS_{148}-*b*-PFAA-$DOPO_{80}$ self-extinguished quickly after a faint flame appeared at the second ignition. In addition, the combustion time of PS_{148}-*b*-PFAA-$DOPO_{80}$ is significantly shortened (<10s) than that of PS_{148}-Br, and only a small amount of smoke is generated during combustion, reaching the V-0 level of UL-94.

The LOI value (Table 9) of PS-*b*-PFAA-DOPO increased with the increase of FAA-DOPO chains in PS_{148}-Br macromolecular chains, and the LOI value of PS_{148}-*b*-PFAA-$DOPO_{80}$ reached 28.8%, which increased by 59.12% compared with 18.1% of PS_{148}-Br. Generally speaking, materials with an LOI value >26% can be classified as self-extinguishing materials. Therefore, the introduction of FAA-DOPO blocks significantly improved the flame retardancy of PS_{148}-Br. After combustion, phosphorus components pro-

https://doi.org/10.1021/acsomega.3c06235
ACS Omega 2023, 8, 48825−48842

Table 8. TG and DTG Data of PS_{148}-Br, FAA-DOPO, PS_{148}-b-PFAA-$DOPO_{32}$, PS_{148}-b-PFAA-$DOPO_{50}$, and PS_{148}-b-PFAA-$DOPO_{80}$

sample	$T_{5\%}$ (°C)	$T_{50\%}$ (°C)	T_{1max} (°C)	T_{2max} (°C)	residues at 550 °C (%)
PS_{148}-Br	359.22	413.71	419.22		1.36
FAA-DOPO	250.49	405.98	280.49	411.49	9.27
PS_{148}-*b*-PFAA-$DOPO_{32}$	255.39	408.11	265.69	425.73	3.07
PS_{148}-*b*-PFAA-$DOPO_{50}$	270.47	416.41	264.61	418.61	2.81
PS_{148}-*b*-PFAA-$DOPO_{80}$	299.35	380.86	271.82	386.17	7.64

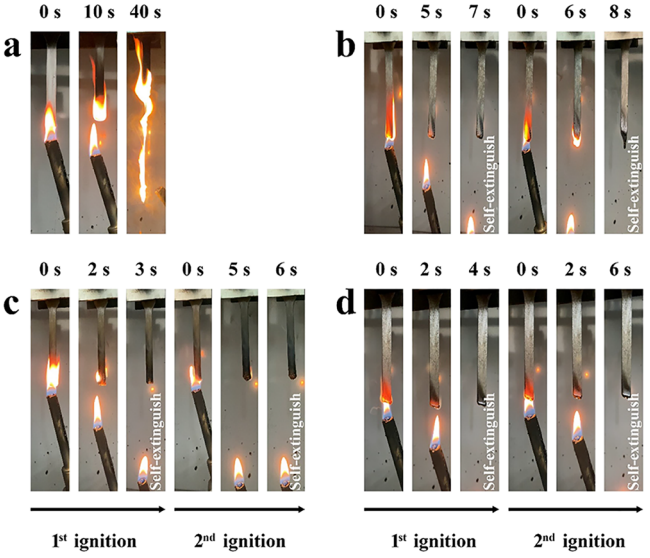

Figure 16. Digital pictures of PS_{148}-Br (a), PS_{148}-*b*-PFAA-$DOPO_{32}$ (b), PS_{148}-*b*-PFAA-$DOPO_{50}$, (c) and PS_{148}-*b*-PFAA-$DOPO_{80}$ (d) during UL-94 tests.

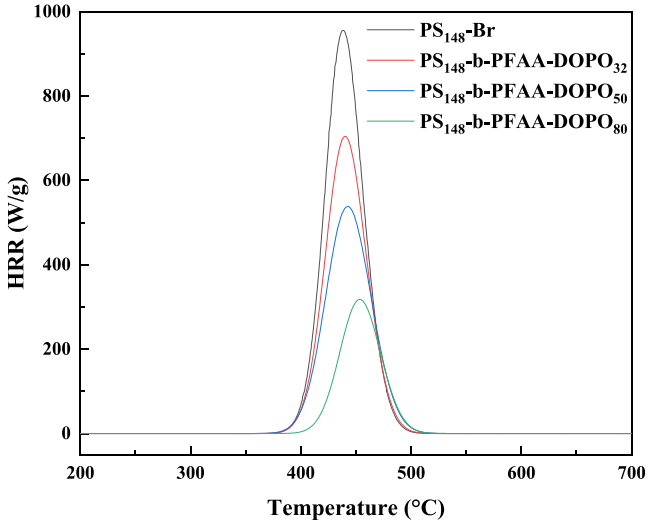

Figure 17. HRR curves of PS_{148}-Br, PS_{148}-*b*-PFAA-$DOPO_{32}$, PS_{148}-*b*-PFAA-$DOPO_{50}$, and PS_{148}-*b*-PFAA-$DOPO_{80}$ test splines.

moted the carbonization and dehydration of PS macromolecules and formed a more continuous and compact carbon layer, which effectively prevented in the gas phase, the generation of PO· and PO_2· radicals can effectively capture H· and HO· active radicals produced in the combustion environment, and enhance the flame suppression effect.[33,69−73]

The combustion behavior of PS-*b*-PFAA-DOPO composites was further investigated via microscale combustion calorimetry (MCC). The results are listed in Figure 17. The peak heat release rate (pHRR) of PS_{148}-Br is as high as 955.8 W/g. After introducing FAA-DOPO segments into the macromolecular chain of PS_{148}-Br, the pHRR of PS-*b*-PFAA-DOPO decreases with the increase of FAA-DOPO segments, and the pHRR of PS_{148}-*b*-PFAA-$DOPO_{80}$ is the lowest, which is 317.8 W/g, which is 66.75% lower than that of PS_{148}-Br. THR of PS-*b*-PFAA-DOPO decreases with the increase of the FAA-DOPO segment, which indicates that the introduction of the FAA-DOPO segment into the PS_{148}-Br macromolecular chain can reduce the heat release rate of PS_{148}-Br to a great extent. In a word, the introduction of the FAA-DOPO segment can reduce the heat release rate of PS_{148}-Br, thus improving the flame retardancy of PS_{148}-Br.

3.5. Analysis of Char Residues. Figure 18 shows the FTIR spectra of char residues after PS_{148}-Br and PS-*b*-PFAA-DOPO combustion. It can be seen from Figure 18 that the FTIR spectra of PS_{148}-*b*-PFAA-$DOPO_{32}$, PS_{148}-*b*-PFAA-$DOPO_{50}$, and PS_{148}-*b*-PFAA-$DOPO_{80}$ after combustion are almost the same. The FTIR of PS_{148}-*b*-PFAA-$DOPO_{32}$, PS_{148}-*b*-PFAA-$DOPO_{50}$, and PS_{148}-*b*-PFAA-$DOPO_{80}$ after combustion have peaks at 1120 and 1204 cm^{-1} belonging to P−O bond and C−O bond respectively, and the P−O peak is significantly smaller than that before combustion (Figure 13). In addition, the FTIR of PS_{148}-*b*-PFAA-$DOPO_{32}$, PS_{148}-*b*-PFAA-$DOPO_{50}$, and PS_{148}-*b*-PFAA-$DOPO_{80}$ char residues after combustion did not have peaks at 928 and 1257 cm^{-1}, which is attributed to P−O bond and P═O, respectively. It can be seen that the P−O bond and P═O bond break during combustion.

Figure 19 shows SEM photos of char residues after PS_{148}-Br and PS-*b*-PFAA-DOPO combustion. As can be seen from Figure 19, the char residues of PS_{148}-Br are thin,

Table 9. UL-94, LOI, and MCC of PS_{148}-Br and PS-b-PFAA-DOPO[a]

sample	UL-94	LOI (%)	HRC (J g^{-1} K^{-1})	pHRR (W g^{-1})	THR (kJ g^{-1})	T_p (°C)
PS_{148}-Br	N/A	18.1	1028	955.8	42.4	438.7
PS_{148}-*b*-PFAA-$DOPO_{32}$	V-0	19.6	781	704.5	35.4	440.2
PS_{148}-*b*-PFAA-$DOPO_{50}$	V-0	24.3	642	538.3	30.2	442.4
PS_{148}-*b*-PFAA-$DOPO_{80}$	V-0	28.8	331	317.8	16.3	453.6

[a]Abbreviations: HRC, heat release capacity; pHRR, peak heat release rate; THR, total heat release; and T_p, temperature of pHRR.

https://doi.org/10.1021/acsomega.3c06235
ACS Omega 2023, 8, 48825−48842

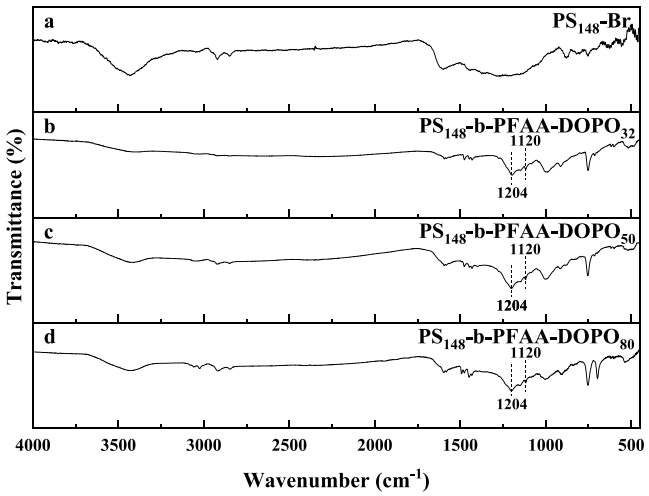

Figure 18. FTIR of char residue of PS_{148}-Br (a), PS_{148}-*b*-PFAA-$DOPO_{32}$ (b), PS_{148}-*b*-PFAA-$DOPO_{50}$ (c), and PS_{148}-*b*-PFAA-$DOPO_{80}$ (d).

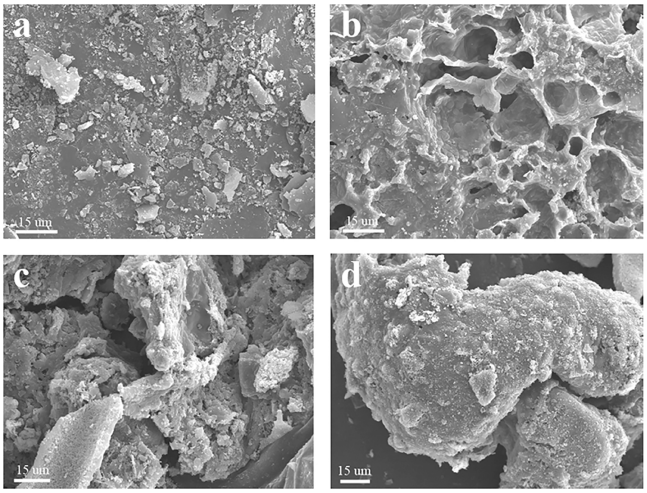

Figure 19. SEM images of char residue of PS_{148}-Br (a), PS_{148}-*b*-PFAA-$DOPO_{32}$ (b), PS_{148}-*b*-PFAA-$DOPO_5$ (c), and PS_{148}-*b*-PFAA-$DOPO_{80}$ (d).

discontinuous patches, whereas the residues of PS_{148}-*b*-PFAA-$DOPO_{32}$, PS_{148}-*b*-PFAA-$DOPO_{50}$, and PS_{148}-*b*-PFAA-$DOPO_{80}$ are thick, continuous patches.

FTIR and SEM analysis of PS_{148}-Br and PS-*b*-PFAA-DOPO after combustion showed that the FAA-DOPO block was introduced into the polystyrene macromolecular chain; during the combustion of PS-*b*-PFAA-DOPO, the DOPO groups degrade to produce phosphoric acid and polyphosphoric acid, which can accelerate the dehydration of polystyrene and promote the carbonization behavior of polystyrene. Meanwhile, the PO· and PO_2· radicals produced by the combustion of DOPO groups capture the flame propagating radicals (H· and HO·) to achieve the purpose of flame retardant.[22,33,41,56,59,72−78]

4. CONCLUSIONS

In this study, DOPO-based monomer FAA-DOPO was synthesized, and polystyrene intrinsic flame retardant was synthesized by ATRP technology. PS_{148}-*b*-PFAA-$DOPO_{32}$, PS_{148}-*b*-PFAA-$DOPO_{50}$, and PS_{148}-*b*-PFAA-$DOPO_{80}$ have UL-94 grade up to V-0 grade, and LOI values increased by 8.29, 34.25, and 59.12% compared with PS_{148}-Br, respectively. Phosphorus radicals (PO· and PO_2·) produced by the thermal decomposition of PS_{148}-*b*-PFAA-$DOPO_{32}$ and PS_{148}-*b*-PFAA-$DOPO_{50}$ and PS_{148}-*b*-PFAA-$DOPO_{80}$ capture H· and HO· radicals formed by the combustion of polystyrene macromolecular chains, thus achieving the purpose of extinguishing fire and increasing the thickness and continuity of the carbon layer. This study provides a reference for the preparation of polystyrene intrinsic flame retardant and is expected to promote the further application of living polymerization in the flame retardant field.

AUTHOR INFORMATION

Corresponding Authors

Shaobo Dong − *College of Chemistry and Chemical Engineering, Northeast Petroleum University, Daqing 163318, People's Republic of China; Heilongjiang Province Key Laboratory of Polymeric Composition Material, College of Materials Science and Engineering, Qiqihar University, Qiqihar 161006, People's Republic of China;* orcid.org/0000-0002-9443-3469; Email: dongshaobo1990@163.com

Yazhen Wang − *College of Chemistry and Chemical Engineering, Northeast Petroleum University, Daqing 163318, People's Republic of China; Heilongjiang Province Key Laboratory of Polymeric Composition Material, College of Materials Science and Engineering, Qiqihar University, Qiqihar 161006, People's Republic of China; College of Chemistry, Chemical Engineering and Resource Utilization, Northeast Forestry University, Harbin 150040, People's Republic of China*; Email: wyz6166@nefu.edu.cn

Authors

Li Liu − *College of Chemistry and Chemical Engineering, Qiqihar University, Qiqihar 161006, People's Republic of China*

Hongge Jia − *Heilongjiang Province Key Laboratory of Polymeric Composition Material, College of Materials Science and Engineering, Qiqihar University, Qiqihar 161006, People's Republic of China*

Yu Zang − *Heilongjiang Province Key Laboratory of Polymeric Composition Material, College of Materials Science and Engineering, Qiqihar University, Qiqihar 161006, People's Republic of China;* orcid.org/0000-0001-5123-4251

Liwu Zu − *Heilongjiang Province Key Laboratory of Polymeric Composition Material, College of Materials Science and Engineering, Qiqihar University, Qiqihar 161006, People's Republic of China;* orcid.org/0000-0002-2132-9548

Tianyu Lan − *College of Chemistry and Chemical Engineering, Northeast Petroleum University, Daqing 163318, People's Republic of China; Heilongjiang Province Key Laboratory of Polymeric Composition Material, College of Materials Science and Engineering, Qiqihar University, Qiqihar 161006, People's Republic of China*

Jun Wang − *College of Chemistry and Chemical Engineering, Northeast Petroleum University, Daqing 163318, People's Republic of China*

Complete contact information is available at: https://pubs.acs.org/10.1021/acsomega.3c06235

https://doi.org/10.1021/acsomega.3c06235
ACS Omega 2023, 8, 48825−48842

Author Contributions

[⊥]S.D. and Y.W. contributed equally to this work.

Notes

The authors declare no competing financial interest.

■ ACKNOWLEDGMENTS

We thank the Heilongjiang Province Key Laboratory of Polymeric Composition Material for its support. This work was financially supported by The Fundamental Research Funds in Heilongjiang Provincial Universities (Nos. 145209301, 135309110).

■ REFERENCES

(1) Chen, Y.; Feng, Q.; Nie, Y.; Zhang, J.; Yang, L. A Review of Combustion and Flame Spread over Thermoplastic Materials: Research Advances and Prospects. *Fire-Basel* **2023**, *6* (3), No. 125.

(2) Quan, Y.; Zhang, Z.; Tanchak, R. N.; Wang, Q. A review on cone calorimeter for assessment of flame-retarded polymer composites. *J. Therm. Anal. Calorim.* **2022**, *147* (19), 10209−10234.

(3) Baby, A.; Tretsiakova-McNally, S.; Arun, M.; Joseph, P.; Zhang, J. Reactive and Additive Modifications of Styrenic Polymers with Phosphorus-Containing Compounds and Their Effects on Fire Retardance. *Molecules* **2020**, *25* (17), No. 3779.

(4) Weil, E. D.; Levchik, S. V. Flame Retardants for Polystyrenes in Commercial Use or Development. *J. Fire Sci.* **2007**, *25* (3), 241−265.

(5) Joseph, P.; Tretsiakova-McNally, S. Melt-Flow Behaviours of Thermoplastic Materials under Fire Conditions: Recent Experimental Studies and Some Theoretical Approaches. *Materials* **2015**, *8* (12), 8793−8803.

(6) Price, D.; Cunliffe, L. K.; Bullett, K. J.; Hull, T. R.; Milnes, G. J.; Ebdon, J. R.; Hunt, B. J.; Joseph, P. Thermal behaviour of covalently bonded phosphate and phosphonate flame retardant polystyrene systems. *Polym. Degrad. Stab.* **2007**, *92* (6), 1101−1114.

(7) Wang, N.; Tu, R.; Ma, X.; Xie, Q.; Jiang, X. Melting behavior of typical thermoplastic materials − An experimental and chemical kinetics study. *J. Hazard. Mater.* **2013**, *262*, 9−15.

(8) Vahabi, H.; Laoutid, F.; Mehrpouya, M.; Saeb, M. R.; Dubois, P. Flame retardant polymer materials: An update and the future for 3D printing developments. *Mater. Sci. Eng. R.* **2021**, *144*, No. 100604.

(9) Levchik, S. V.; Weil, E. D. New developments in flame retardancy of styrene thermoplastics and foams. *Polym. Int.* **2008**, *57* (3), 431−448.

(10) Zhou, H.; Wen, D.; Hao, X.; Chen, C.; Zhao, N.; Ou, R.; Wang, Q. Nanostructured multifunctional wood hybrids fabricated via in situ mineralization of zinc borate in hierarchical wood structures. *Chem. Eng. J.* **2023**, *451*, No. 138308.

(11) Zhu, G.; Li, H.; Deng, S.; Zhang, C.; Kang, K. A multifunctional ZnO-ZIF-8/bamboo composite with enhanced adsorption capacity and improved flame retardancy. *Wood Mater. Sci. Eng.* **2023**, *18* (3), 902−909.

(12) Zhu, D.; Bi, Q.; Yin, G.; Jiang, Y.; Fu, W.; Wang, N.; Wang, D. Investigation of magnesium hydroxide functionalized by polydopamine/transition metal ions on flame retardancy of epoxy resin. *J. Therm. Anal. Calorim.* **2022**, *147* (23), 13301−13312.

(13) Liu, Y.; Yu, Z.; Lu, G.; Chen, W.; Ye, Z.; He, Y.; Tang, Z.; Zhu, J. Versatile levulinic acid-derived dynamic covalent thermosets enabled by in situ generated imine and multiple hydrogen bonds. *Chem. Eng. J.* **2023**, *451*, No. 139053.

(14) Zhu, Y.; Wu, W.; Xu, T.; Xu, H.; Zhong, Y.; Zhang, L.; Ma, Y.; Sui, X.; Wang, B.; Feng, X.; Mao, Z. Effect of weak intermolecular interactions in micro/nanoscale polyphosphazenes and polyethylene terephthalate composites on flame retardancy. *Polym. Adv. Technol.* **2022**, *33* (7), 2231−2243.

(15) Zhu, Y.; Wu, W.; Xu, T.; Xu, H.; Zhong, Y.; Zhang, L.; Ma, Y.; Sui, X.; Wang, B.; Feng, X.; Mao, Z. Preparation and characterization of polyphosphazene-based flame retardants with different functional groups. *Polym. Degrad. Stab.* **2022**, *196*, No. 109815.

(16) Zhou, X.; Yu, R.; Jiang, J.; Dang, J.; Luan, J.; Wang, G.; Zhang, M. PEEK composite resin with enhanced intumescent flame retardancy loaded with Octaphenylsilsesquioxane and nano calcium carbonate and its application in fibers. *Polym. Degrad. Stab.* **2022**, *202*, No. 110042.

(17) Zhang, W.; Huang, J.; Guo, X.; Zhang, W.; Qian, L.; Qin, Z. Double organic groups-containing polyhedral oligomeric silsesquioxane filled epoxy with enhanced fire safety. *J. Appl. Polym. Sci.* **2022**, *139* (26), No. 52461.

(18) Lyu, B.; Kou, M.; Gao, D.; Luo, K.; Ma, J.; Lin, Y. Flame retardancy of carboxylated polyhedral oligosilsesquioxane modified layered double hydroxide in the process of leather fatliquoring. *J. Appl. Polym. Sci.* **2022**, *139* (27), No. 52468.

(19) Solihat, N. N.; Hidayat, A. F.; Taib, M. N. A. M.; Hussin, M. H.; Lee, S. H.; Ghani, M. A. A.; Edrus, S. S. O. A.; Vahabi, H.; Fatriasari, W. Recent developments in flame-retardant lignin-based biocomposite: manufacturing, and characterization. *J. Polym. Environ.* **2022**, *30* (11), 4517−4537.

(20) Li, X.; Shi, X.; Chen, M.; Liu, Q.; Li, Y.; Li, Z.; Huang, Y.; Wang, D. Biomass-based coating from chitosan for cotton fabric with excellent flame retardancy and improved durability. *Cellulose* **2022**, *29* (9), 5289−5303.

(21) Xu, J.; Niu, Y.; Xie, Z.; Liang, F.; Guo, F.; Wu, J. Synergistic flame retardant effect of carbon nanohorns and ammonium polyphosphate as a novel flame retardant system for cotton fabrics. *Chem. Eng. J.* **2023**, *451*, No. 138566.

(22) Jiang, G.; Xiao, Y.; Qian, Z.; Yang, Y.; Jia, P.; Song, L.; Hu, Y.; Ma, C.; Gui, Z. A novel phosphorus-, nitrogen- and sulfur-containing macromolecule flame retardant for constructing high-performance epoxy resin composites. *Chem. Eng. J.* **2023**, *451*, No. 137823.

(23) Zhu, Y.; Cai, W.; Zhao, Y.; Mu, X.; Zhou, X.; Chu, F.; Wang, B.; Hu, Y. Graphite-like carbon nitride/polyphosphoramide nanohybrids for enhancement on thermal stability and flame retardancy of thermoplastic polyurethane elastomers. *ACS Appl. Polym. Mater.* **2022**, *4* (1), 121−128.

(24) Zhou, W.; Lv, D.; Ding, H.; Xu, P.; Zhang, C.; Ren, Y.; Yang, W.; Ma, P. Synthesis of eugenol-based phosphorus-containing epoxy for enhancing the flame-retardancy and mechanical performance of DGEBA epoxy resin. *React. Funct. Polym.* **2022**, *180*, No. 105383.

(25) Tan, W.; Ren, Y.; Guo, Y.; Liu, Y.; Liu, X.; Qu, H. A novel multi-claw reactive flame retardant derived from DOPO for endowing lyocell fabric with high effective flame retardancy. *Cellulose* **2022**, *29* (12), 6941−6962.

(26) Ma, L.; Liu, H.; Wen, X.; Szymańska, K.; Mijowska, E.; Hao, C.; Tang, T.; Lei, Q. Polyhydric SiO_2 coating assistant to graft organophosphorus onto glass fabric for simultaneously improving flame retardancy and mechanical properties of epoxy resin composites. *Compos. Part B-Eng.* **2022**, *243*, No. 110176.

(27) Liu, D.; Zhao, W.; Cui, Y.; Zhang, T.; Ji, P. Influence of the chemical structure on the flame retardant mechanism and mechanical properties of flame-retardant epoxy resin thermosets. *Macromol. Mater. Eng.* **2022**, *307* (9), No. 2200169.

(28) Kuhnigk, J.; Standau, T.; Dörr, D.; Brütting, C.; Altstädt, V.; Ruckdäschel, H. Progress in the development of bead foams − A review. *J. Cell. Plast.* **2022**, *58* (4), 707−735.

(29) Rad, E. R.; Vahabi, H.; de Anda, A. R.; Saeb, M. R.; Thomas, S. Bio-epoxy resins with inherent flame retardancy. *Prog. Org. Coat.* **2019**, *135*, 608−612.

(30) D'Silva, K.; Fernandes, A.; Rose, M. Brominated Organic Micropollutants—Igniting the Flame Retardant Issue. *Crit. Rev. Env. Sci. Tec.* **2004**, *34* (2), 141−207.

(31) Feng, J.; Liu, L.; Zhang, Y.; Wang, Q.; Liang, H.; Wang, H.; Song, P. Rethinking the pathway to sustainable fire retardants. *Exploration* **2023**, *3* (4), No. 20220088.

https://doi.org/10.1021/acsomega.3c06235
ACS Omega 2023, 8, 48825−48842

(32) Ren, J.; Huo, S.; Huang, G.; Wang, T.; Feng, J.; Chen, W.; Xiao, S.; Song, P. A novel P/Ni-doped g-C3N4 nanosheets for improving mechanical, thermal and flame-retardant properties of acrylonitrile−butadienestyrene resin. *Chem. Eng. J.* **2023**, *452*, No. 139196.
(33) Zhang, A.; Zhang, J.; Liu, L.; Dai, J.; Lu, X.; Huo, S.; Hong, M.; Liu, X.; Lynch, M.; Zeng, X.; et al. Engineering phosphorus-containing lignin for epoxy biocomposites with enhanced thermal stability, fire retardancy and mechanical properties. *J. Mater. Sci. Technol.* **2023**, *167*, 82−93.
(34) Yao, M.; Liu, L.; Ma, C.; Zhang, H.; Zhang, Y.; Song, R.; Fang, Z.; Song, P. A lysine-derived flame retardant for improved flame retardancy, crystallinity, and aqueous-phase degradation of polylactide. *Chem. Eng. J.* **2023**, *462*, No. 142189.
(35) Xue, Y.; Zhang, T.; Tian, L.; Feng, J.; Song, F.; Pan, Z.; Zhang, M.; Zhou, Y.; Song, P. A molecularly engineered bioderived polyphosphonate containing Schiff base towards fire-retardant PLA with enhanced crystallinity and mechanical properties. *Chem. Eng. J.* **2023**, *472*, No. 144986.
(36) Feng, J.; Lu, Y.; Xie, H.; Zhang, Y.; Huo, S.; Liu, X.; Flynn, M.; Xu, Z.; Burey, P.; Lynch, M.; et al. Atom-economic synthesis of an oligomeric P/N-containing fire retardant towards fire-retarding and mechanically robust polylactide biocomposites. *J. Mater. Sci. Technol.* **2023**, *160*, 86−95.
(37) Vahabi, H.; Laoutid, F.; Formela, K.; Saeb, M. R.; Dubois, P. Flame-retardant polymer materials developed by reactive extrusion: present status and future perspectives. *Polym. Rev.* **2022**, *62* (4), 919−949.
(38) Velencoso, M. M.; Battig, A.; Markwart, J. C.; Schartel, B.; Wurm, F. R. Molecular Firefighting—How Modern Phosphorus Chemistry Can Help Solve the Challenge of Flame Retardancy. *Angew. Chem., Int. Ed.* **2018**, *57* (33), 10450−10467.
(39) Schartel, B. Phosphorus-based Flame Retardancy Mechanisms-Old Hat or a Starting Point for Future Development? *Materials* **2010**, *3* (10), 4710−4745.
(40) Joseph, P.; Tretsiakova-Mcnally, S. Reactive modifications of some chain- and step-growth polymers with phosphorus-containing compounds: effects on flame retardance-a review. *Polym. Adv. Technol.* **2011**, *22* (4), 395−406.
(41) Hochół, A.; Flejszar, M.; Chmielarz, P. Advances and opportunities in synthesis of flame retardant polymers via reversible deactivation radical polymerization. *Polym. Degrad. Stab.* **2023**, *214*, No. 110414.
(42) Laoutid, F.; Bonnaud, L.; Alexandre, M.; Lopez-Cuesta, J. M.; Dubois, P. New prospects in flame retardant polymer materials: From fundamentals to nanocomposites. *Mater. Sci. Eng. R.* **2009**, *63* (3), 100−125.
(43) Liu, B. W.; Zhao, H. B.; Wang, Y. Z. Advanced Flame-Retardant Methods for Polymeric Materials. *Adv. Mater.* **2022**, *34* (46), No. 2107905.
(44) Luo, H.; Liu, C.; He, D.; Xu, J.; Sun, J.; Li, J.; Pan, X. Environmental behaviors of microplastics in aquatic systems: A systematic review on degradation, adsorption, toxicity and biofilm under aging conditions. *J. Hazard. Mater.* **2022**, *423*, No. 126915.
(45) Dong, S.; Wang, Y.; Lan, T.; Wang, J.; Zu, L.; Xiao, T.; Yang, Y.; Wang, J. Synthesis of High-Molecular-Weight Bifunctional Additives with both Flame Retardant Properties and Antistatic Properties via ATRP. *ACS Omega* **2022**, *7* (48), 44287−44297.
(46) Chingsheng, C.; Leowang, C.; Yieshun, C. Novel flame retardant epoxy resins - I: Synthesis, characterization, and properties of aryl phosphinate epoxy ether cured with diamine. *Polym. Bull.* **1998**, *41* (1), 45−52.
(47) Chunshan, W.; Chinghsuan, L. Synthesis and properties of phosphorus-containing epoxy resins by novel method. *J. Polym. Sci., Part A: Polym. Chem.* **1999**, *37* (21), 3903−3909.
(48) Lin, C. H.; Wu, C. Y.; Wang, C. S. Synthesis and properties of phosphorus-containing advanced epoxy resins II. *J. Appl. Polym. Sci.* **2000**, *78* (1), 228−235.
(49) José, A. M.; Alejandro, E. M.; Marina, G.; Virginia, C. Synthesis, characterization and polymerization of a novel glycidyl phosphinate. *Macromol. Rapid Commun.* **2001**, *22* (15), 1265−1271.
(50) Liu, Y. L.; Wu, C. S.; Hsu, K. Y.; Chang, T. C. Flame-retardant epoxy resins from o-cresol novolac epoxy cured with a phosphorus-containing aralkyl novolac. *J. Polym. Sci., Polym. Chem.* **2002**, *40* (14), 2329−2339.
(51) Yingling, L.; Chuanshao, W.; Yieshun, C.; Wenhsuan, H. Preparation, thermal properties, and flame retardance of epoxy-silica hybrid resins. *J. Polym. Sci., Pat A: Polym. Chem.* **2003**, *41* (15), 2354−2367.
(52) Wang, X.; Zhang, Q. Synthesis, characterization, and cure properties of phosphorus-containing epoxy resins for flame retardance. *Eur. Polym. J.* **2004**, *40* (2), 385−395.
(53) Wang, Y. C.; Li, F.; Zhao, J. P. Novel halogen-free Si-C-P flame-retarding coatings constructed by DOPO/flake graphite co-doping silica fume-based geopolymer. *J. Appl. Polym. Sci.* **2023**, *140* (12), No. 53645.
(54) Zhou, Y.; Hu, Q.; Wang, W.; Wang, R. Controlled architecture of polyhedral oligomeric silsesquioxane-functionalized poly(glycidyl methacrylate)/polyester composites using surface-initiated ICAR ATRP Technique for High Flame Retardancy and Smoke Suppression. *Polym. Degrad. Stab.* **2022**, *199*, No. 109914.
(55) Zhou, R.; Lin, L.; Zeng, B.; Yi, X.; Huang, C.; Du, K.; Liu, X.; Xu, Y.; Yuan, C.; Dai, L. Diblock Copolymers Containing Titanium-Hybridized Polyhedral Oligomeric Silsesquioxane Used as a Macromolecular Flame Retardant for Epoxy Resin. *Polymers-Basel* **2022**, *14* (9), No. 1708.
(56) Zhao, Z.; Wang, J.; Wang, J.; Chen, K.; Zhang, B.; Chen, Q.; Guo, P.; Wang, X.; Liu, F.; Huo, S.; Yang, S. Facile fabrication of single-component flame-retardant epoxy resin with rapid curing capacity and satisfied thermal resistance. *React. Funct. Polym.* **2022**, *170*, No. 105103.
(57) Zhao, Z.; Tan, Y.; Guo, S.; Ni, X. An efficient composite modifier prepared for enhancing the crystallization and flame-retardancy of poly(m-xylylene adipamide). *Polymers-Basel* **2022**, *14* (17), No. 3626.
(58) Zhao, W.; Zhao, H.-B.; Cheng, J.-B.; Li, W.; Zhang, J.; Wang, Y.-Z. A green, durable and effective flame-retardant coating for expandable polystyrene foams. *Chem. Eng. J.* **2022**, *440*, No. 135807.
(59) Zhao, W.; Wang, J.; Zhuang, G.; Liu, D.; Sun, C. Thermal stability and flame retardancy of epoxy resin with DOPO-based compound containing triazole and hydroxyl groups. *Macromol. Mater. Eng.* **2022**, *307* (11), No. 2200408.
(60) Zhang, Q.; Liu, H.; Guan, J.; Yang, X.; Luo, B. Synergistic Flame Retardancy of Phosphatized Sesbania Gum/Ammonium Polyphosphate on Polylactic Acid. *Molecules* **2022**, *27* (15), No. 4748.
(61) Huang, W.; Wang, K.; Tu, C.; Xu, X.; Tian, Q.; Ma, C.; Fu, Q.; Yan, W. Synergistic Effects of DOPO-Based Derivative and Organo-Montmorillonite on Flame Retardancy, Thermal Stability and Mechanical Properties of Polypropylene. *Polymers-Basel* **2022**, *14* (12), No. 2372.
(62) Yu, B.; Yuen, A. C. Y.; Xu, X.; Zhang, Z.; Yang, W.; Lu, H.; Fei, B.; Yeoh, G. H.; Song, P.; Wang, H. Engineering MXene surface with POSS for reducing fire hazards of polystyrene with enhanced thermal stability. *J. Hazard. Mater.* **2021**, *401*, No. 123342.
(63) Zhang, Y.; Yu, B.; Wang, B.; Liew, K. M.; Song, L.; Wang, C.; Hu, Y. Highly Effective P−P Synergy of a Novel DOPO-Based Flame Retardant for Epoxy Resin. *Ind. Eng. Chem. Res.* **2017**, *56* (5), 1245−1255.
(64) Tang, S.; Qian, L.; Liu, X.; Dong, Y. Gas-phase flame-retardant effects of a bi-group compound based on phosphaphenanthrene and triazine-trione groups in epoxy resin. *Polym. Degrad. Stab.* **2016**, *133*, 350−357.
(65) Qian, L.; Qiu, Y.; Wang, J.; Xi, W. High-performance flame retardancy by char-cage hindering and free radical quenching effects in epoxy thermosets. *Polymer* **2015**, *68*, 262−269.

https://doi.org/10.1021/acsomega.3c06235
ACS Omega 2023, 8, 48825−48842

(66) Perret, B.; Schartel, B.; Stöß, K.; Ciesielski, M.; Diederichs, J.; Döring, M.; Krämer, J.; Altstädt, V. Novel DOPO-based flame retardants in high-performance carbon fibre epoxy composites for aviation. *Eur. Polym. J.* **2011**, *47* (5), 1081−1089.
(67) Schartel, B.; Braun, U.; Balabanovich, A. I.; Artner, J.; Ciesielski, M.; Döring, M.; Perez, R. M.; Sandler, J. K. W.; Altstädt, V. Pyrolysis and fire behaviour of epoxy systems containing a novel 9,10-dihydro-9-oxa-10-phosphaphenanthrene-10-oxide-(DOPO)-based diamino hardener. *Eur. Polym. J.* **2008**, *44* (3), 704−715.
(68) Schäfer, A.; Seibold, S.; Lohstroh, W.; Walter, O.; Döring, M. Synthesis and properties of flame-retardant epoxy resins based on DOPO and one of its analog DPPO. *J. Appl. Polym. Sci.* **2007**, *105* (2), 685−696.
(69) Wang, Y.; Qing, Y.; Sun, Y.; Zhu, M.; Dong, S. A study on preparation of modified Graphene Oxide and flame retardancy of polystyrene composite microspheres. *Des. Monomers Polym.* **2020**, *23* (1), 1−15.
(70) Lu, X.; Lee, A. F.; Gu, X. Improving the flame retardancy of sustainable lignin-based epoxy resins using phosphorus/nitrogen treated cobalt metal-organic frameworks. *Mater. Today Chem.* **2022**, *26*, No. 101184.
(71) Lu, X.; Gu, X. Fabrication of a bi-hydroxyl-bi-DOPO compound with excellent quenching and charring capacities for lignin-based epoxy resin. *Int. J. Biol. Macromol.* **2022**, *205*, 539−552.
(72) Yang, Y.; Li, Z.; Wu, G.; Chen, W.; Huang, G. A novel biobased intumescent flame retardant through combining simultaneously char-promoter and radical-scavenger for the application in epoxy resin. *Polym. Degrad. Stab.* **2022**, *196*, No. 109841.
(73) Teng, N.; Dai, J.; Wang, S.; Hu, J.; Liu, X. Hyperbranched flame retardant for epoxy resin modification: Simultaneously improved flame retardancy, toughness and strength as well as glass transition temperature. *Chem. Eng. J.* **2022**, *428*, No. 131226.
(74) Zhu, K.; Jiang, Z.; Xu, X.; Zhang, Y.; Zhu, M.; Wang, J.; Ren, A. Preparation and thermal cross-linking mechanism of co-polyester fiber with flame retardancy and anti-dripping by in situ polymerization. *RSC Adv.* **2021**, *12* (1), 168−180.
(75) Zhang, A.; Wang, W.; Dong, Z.; Wei, J.; Wei, L.; Gu, W.; Zheng, G.; Wang, R. Mechanical, Thermal Stability, and Flame Retarding Properties of Phosphorus-Modified PET Blended with DOPO-POSS. *ACS Omega* **2022**, *7* (50), 46277−46287.
(76) Yang, Y.; Chen, W.; Li, Z.; Huang, G.; Wu, G. Efficient flame retardancy, good thermal stability, mechanical enhancement, and transparency of DOPO-conjugated structure compound on epoxy resin. *Chem. Eng. J.* **2022**, *450*, No. 138424.
(77) Xu, J.; Yang, H.; Luo, Z.; Wu, D.; Cao, G. Synergistic effects of core@double-shell structured magnesium hydroxide microcapsules on flame retardancy and smoke suppression in flexible poly(vinyl chloride). *RSC Adv.* **2022**, *12* (5), 2914−2927.
(78) Wen, M.; Xu, J.; Zhu, J.; Liu, Y.; Deng, C.; Shi, J.; Park, H. Preparation of bisDOPO-NH2-POSS flame retardant and its application to plywood using modified urea-formaldehyde resin. *Wood Mater. Sci. Eng.* **2023**, *18* (4), 1252−1263.

https://doi.org/10.1021/acsomega.3c06235
ACS Omega 2023, 8, 48825−48842